Eur. Phys. J. C 56, 407–423 (2008)
DOI 10.1140/epjc/s10052-008-0656-9

THE EUROPEAN PHYSICAL JOURNAL C

Regular Article – Theoretical Physics

Perturbative photon fluxes generated by high-frequency gravitational waves and their physical effects

Fangyu Li[1,a], R.M.L. Baker Jr.[2,b], Zhenyun Fang[1,c], G.V. Stephenson[3,d], Zhenya Chen[1,e]

[1] Department of Physics, Chongqing University, Chongqing 400044, P.R. China
[2] GRAWAVE® LLC, 8123 Tuscany Avenue, Playa del Rey, CA 90293, USA
[3] Seculine Consulting, P.0. Box 925, Redondo Beach, CA 90277, USA

Received: 17 January 2008 / Revised version: 2 June 2008 /
Published online: 8 July 2008 –

Abstract. We consider the electromagnetic (EM) perturbative effects produced by high-frequency gravitational waves (HFGWs) in the GHz band in a special EM resonance system, which consists of fractal membranes, a Gaussian beam (GB) passing through a static magnetic field. Under the synchro-resonance condition, coherence modulation of the HFGWs to the preexisting transverse components of the GB is predicted to produce the transverse perturbative photon flux (PPF), which has three novel and important properties. (1) The PPF has a maximum at a longitudinal symmetrical surface of the GB where the transverse background photon flux (BPF) vanishes; (2) the resonant effect will be high sensitive to the propagating directions of the HFGWs; (3) the PPF reflected or transmitted by the fractal membrane exhibits a very small decay to be compared with a very large decay of the much stronger BPF. Such properties might provide a new way to distinguish and display the perturbative effects produced by the HFGWs. We also discuss the high-frequency asymptotic behavior of the relic GWs in the microwave band and the positive definite issues of their energy-momentum pseudo-tensor.

PACS. 04.30.Nk; 04.25.Nx; 04.30.Db; 98.80.Cq

1 Introduction

Unlike the usual celestial gravitational waves (GWs), having low frequencies, which are often a small fraction of a Hz, the relic GWs in the microwave band ($\sim 10^8$–10^{11} Hz), predicted by the quintessential inflationary models (QIM) [1–3], the pre-big bang scenario (PBBS) and some string cosmology scenarios [4–7], form high-frequency random signals, and the root-mean-square (r.m.s.) values of the dimensionless amplitudes might reach up to $\sim 10^{-30}$–$10^{-33}/\sqrt{\text{Hz}}$, and because of their weakness and very high-frequency properties, they are quite different from low-frequency GWs. The thermal motion of plasma of stars, the interaction of the EM waves with interstellar plasma and magnetic fields, the evaporation of primordial black holes [8], even ultra-high-intensity lasers [9] and other high-energy laboratory schemes [10–12] are possible means to generate the HFGWs in the GHz band and higher frequencies. Interaction of the HFGWs with the EM fields and the EM detection of the HFGWs have been theoretically and experimentally studied by many authors [13–38]. These works include gravitation–EM conversion in static EM fields (e.g., the Gertsenshtein effect and its inverse effect), the cavity classical- and cavity quantum-electrodynamical response to the HFGWs, resonant photon–graviton conversion, Berry's phase in the EM detection of the HFGWs, resonant interaction of the HFGWs with the EM wave beams, rotation of the polarization vector of EM wave caused by the HFGWs in the toroidal waveguide, difference in frequency resonant response of coupled spherical cavities, etc.

Although the relic GWs have not yet been detected, we can be reasonably sure that the earth is bathed in a sea of these relic GWs. Since 1978 such relic and primordial background GWs have been of ever increasing scientific interest as many researches have shown [39–43].

Based on high-dimensional (bulk) spacetime theories, it has also theoretically been shown [44, 45] that all familiar matter fields are constrained to live on our brane world, while gravity is free to propagate in the extra dimensions, and the HFGWs (i.e., high-energy gravitons) would be more capable of carrying energy from our 3-brane world than lower-frequency GWs. It is noted that propagation of the HFGWs may be a unique and effective way for exchanging energy and information between two adjacent parallel brane worlds [46–49]. Moreover, if the pre-big

[a] e-mail: cqufangyuli@hotmail.com
[b] e-mail: DrRobertBaker@GravWave.com
[c] e-mail: zyfang@cqu.edu.cn
[d] e-mail: seculine@gmail.com
[e] e-mail: ccjaazz@yahoo.com.cn

bang scenario is correct, then the relic GWs would be an almost unique window from which one can look back into the universe before the big bang [6, 7, 50]. Although these theories and scenarios may be controversial and whether or not they include a fatal flaw remains to be determined. The successful detection of the high-frequency relic gravitational waves (HFRGWs) will certainly shed light on many of these theories.

In this paper we shall discuss some ideas and a theoretical basis for the selection and detection of the HFGWs with the predicted typical parameters $\nu_g \sim 5\times10^9$ Hz (5 GHz) and $h_{\mathrm{r.m.s.}} \sim 10^{-30}$–$10^{-33}/\sqrt{\mathrm{Hz}}$ [1–7, 39–41]. This paper includes the following seven parts: an Introduction; next the asymptotic behavior of the relic GWs in the high-frequency (the microwave band) region and positive definite issues of the energy-momentum pseudo-tensor of the HFRGWs is treated. The EM resonant system to the HFRGWs, i.e., the coupling system of the fractal membranes and a Gaussian beam (GB) passing through a static magnetic field is considered; subsequently we look at the EM resonant response to the HFRGWs and some numerical estimations. In the next section we treat the selection and detection of the PPFs; this is followed by a section with a very brief review of noise issues; finally, we make concluding remarks.

2 The high-frequency relic gravitational waves in the GHz band

2.1 High-frequency asymptotic behavior of the relic GW in the microwave band

It is well known that each polarization component $h_{ij}(\eta,\mathbf{x})$ of the relic GW can be written as [1, 2, 51]

$$h_{ij} = \frac{\mu(\eta)}{a}\exp(\mathrm{i}\mathbf{k}\cdot\mathbf{x})e_{ij}\,, \tag{1}$$

The time dependence of h is determined by the $\mu(\eta)$, satisfying the equation

$$\ddot{\mu} + (k^2 - \ddot{a}/a)\mu = 0\,, \tag{2}$$

where $\ddot{a} = \frac{\partial^2 a}{\partial\eta^2}$, $a = a(\eta)$ is the cosmology scale factor, η is the conformal time. In fact, (2) has different exact solutions [52, 53] in the different evolution stages of the Universe, and their analytic forms are often very complicated. Fortunately, for HFRGWs in the GHz band (i.e., the relic gravitons of large momentum), we have $k^2 \gg |\ddot{a}/a|$ in (2), i.e., a term $\ddot{a}/a$ can be neglected, and then the solution forms can be greatly simplified. In this case (2) has the usual periodic solution

$$\mu(\eta) = A_1(k)\exp(-\mathrm{i}k\eta) + A_2(k)\exp(\mathrm{i}k\eta)\,. \tag{3}$$

By using (1) and (3), we have

$$\begin{aligned} h = {} & A_1(k)/a(\eta)\exp[\mathrm{i}(\mathbf{k}\cdot\mathbf{x} - k\eta)] \\ & + A_2(k)/a(\eta)\exp[\mathrm{i}(\mathbf{k}\cdot\mathbf{x} + k\eta)]\,, \end{aligned} \tag{4}$$

Consequentially, the HFRGWs can be seen as a superposition of all "monochromatic components", (4).

2.2 The positive definite issues of the energy-momentum pseudo-tensor of the HFRGWs

If the relic GWs do exist and have an observable effect, they should obey reasonable expressions for their energy-momentum pseudo-tensor (EMPT). In particular, the energy density of the relic GWs should be positive definite, and the momentum density components should have a reasonable physical behavior. Although the energy spectrum of the relic GWs and their imprint on the cosmic microwave background have been much discussed, there is little research into the complete forms of the EMPT of the relic GWs [3, 54]; this research may provide a theoretical basis for the existence of relic GWs and their detection. Unlike previous works, our attention will only be focused on the EMPT of the HFRGWs in the GHz band, especially the positive definite property of the energy density of them.

The relic GWs are small corrections to the background metric tensor, the spacetime background is the de Sitter spacetime, and the metric takes the form [39–41]

$$\mathrm{d}s^2 = a^2(\eta)\left[-\mathrm{d}\eta^2 + (\delta_{ij} + h_{ij})\mathrm{d}x^i\,\mathrm{d}x^j\right] = g_{\mu\nu}\,\mathrm{d}x^\mu\,\mathrm{d}x^\nu\,, \tag{5}$$

$$g_{\mu\nu} = \bar{g}_{\mu\nu} + a^2 h_{\mu\nu}\,, \tag{6}$$

where

$$\bar{g}_{\mu\nu} = (-a^2, a^2, a^2, a^2)\,; \tag{7}$$

δ_{ij} is Kronecker symbol. Because the sea of HFRGWs can be seen as superposition of all "monochromatic components" of the Fourier expansion, each "monochromatic component", (4), contains every possible propagating direction. In this case, we consider a single "monochromatic wave" propagating along the z-axis in Cartesian coordinates without loss of generality. From (5)–(7), the metric has the following form in Cartesian coordinates:

$$g_{\mu\nu} = \begin{pmatrix} -a^2 & 0 & 0 & 0 \\ 0 & a^2(1+h_\oplus) & a^2 h_\otimes & 0 \\ 0 & a^2 h_\otimes & a^2(1-h_\oplus) & 0 \\ 0 & 0 & 0 & a^2 \end{pmatrix}, \tag{8}$$

From (8), we have

$$\begin{aligned} & g_{00} = -a^2\,, && g_{11} = a^2(1+h_\oplus)\,, \\ & g_{22} = a^2(1-h_\oplus)\,, && g_{33} = a^2\,, \\ & g_{12} = g_{21} = a^2 h_\otimes\,, \end{aligned} \tag{9}$$

and

$$g = \det(g_{\mu\nu}) = a^8\left(h_\oplus^2 + h_\otimes^2 - 1\right). \tag{10}$$

The expressions for the Einstein EMPT are [55]

$$\sqrt{-g}t_\mu^\nu = \frac{c^4}{16\pi G}H_{\mu,\sigma}^{\nu\sigma}\,, \tag{11}$$

where

$$H_{\mu}^{\nu\sigma}=\frac{1}{\sqrt{-g}}g_{\mu\lambda}[-g(g^{\nu\lambda}g^{\sigma\gamma}-g^{\sigma\lambda}g^{\nu\gamma})]_{,\gamma} \tag{12}$$

is the super-potential. Since h^2 terms have been taken into account in the determinant of the metric, see (10), and the EMPT for the gravitational field concerns quadratic terms of h, the $h_{\oplus}^2$ and $h_{\otimes}^2$ terms in the inverse of the metric should also be taken into account. By using (8)–(10) and $g_{\mu\alpha}g^{\alpha\nu}=\delta_{\mu}^{\nu}$, neglecting third- and higher-order infinitely small quantities, we obtain non-vanishing components of $g^{\mu\nu}$ and $H_{\mu}^{\nu\alpha}$ in empty space as follows:

$$\begin{aligned}
&g^{00}=-a^{-2}\,,\qquad g^{11}=a^{-2}(1-h_{\oplus}+h_{\oplus}^2+h_{\otimes}^2)\,,\\
&g^{22}=a^{-2}(1+h_{\oplus}+h_{\oplus}^2+h_{\otimes}^2)\,,\\
&g^{33}=a^{-2}\,,\qquad g^{12}=g^{21}=-a^{-2}h_{\otimes}\,, \qquad (13)\\
&H_0^{03}=-H_0^{30}\\
&\quad=\frac{1}{\sqrt{-g}}g_{00}(-gg^{00}g^{33})_{,3}=-2\mathrm{i}ka^2\big(h_{\oplus}^2+h_{\otimes}^2\big)\,, \qquad (14)\\
&H_1^{01}=-H_1^{10}\\
&\quad=\frac{1}{\sqrt{-g}}g_{11}(gg^{11}g^{00})_{,0}+\frac{1}{\sqrt{-g}}g_{12}(gg^{12}g^{00})_{,0}\\
&\quad=4a\dot{a}-a^2\dot{h}_{\oplus}-2a\dot{a}\big(h_{\oplus}^2+h_{\otimes}^2\big)-a^2(h_{\oplus}\dot{h}_{\oplus}+h_{\otimes}\dot{h}_{\otimes})\,, \qquad (15)\\
&H_1^{02}=-H_1^{20}\\
&\quad=\frac{1}{\sqrt{-g}}g_{11}(gg^{21}g^{00})_{,0}+\frac{1}{\sqrt{-g}}g_{12}(gg^{22}g^{00})_{,0}\\
&\quad=a^2(h_{\otimes}\dot{h}_{\oplus}-h_{\oplus}\dot{h}_{\otimes})-a^2\dot{h}_{\otimes}\,, \qquad (16)\\
&H_1^{13}=-H_1^{31}\\
&\quad=\frac{1}{\sqrt{-g}}g_{11}(-gg^{11}g^{33})_{,3}+\frac{1}{\sqrt{-g}}g_{12}(-gg^{12}g^{33})_{,3}\\
&\quad=-\mathrm{i}ka^2\big(h_{\oplus}+h_{\oplus}^2+h_{\otimes}^2\big)\,, \qquad (17)\\
&H_1^{23}=-H_1^{32}\\
&\quad=\frac{1}{\sqrt{-g}}g_{11}(-gg^{21}g^{33})_{,3}+\frac{1}{\sqrt{-g}}g_{12}(-gg^{22}g^{33})_{,3}\\
&\quad=-\mathrm{i}ka^2h_{\otimes}\,, \qquad (18)\\
&H_2^{01}=-H_2^{10}\\
&\quad=\frac{1}{\sqrt{-g}}g_{21}(gg^{11}g^{00})_{,0}+\frac{1}{\sqrt{-g}}g_{22}(gg^{12}g^{00})_{,0}\\
&\quad=a^2(h_{\oplus}\dot{h}_{\otimes}-\dot{h}_{\oplus}-\dot{h}_{\otimes})\,, \qquad (19)\\
&H_2^{02}=-H_2^{20}\\
&\quad=\frac{1}{\sqrt{-g}}g_{21}(gg^{21}g^{00})_{,0}+\frac{1}{\sqrt{-g}}g_{22}(gg^{22}g^{00})_{,0}\\
&\quad=4a\dot{a}+a^2\dot{h}_{\oplus}-2a\dot{a}\big(h_{\oplus}^2+h_{\otimes}^2\big)-a^2(h_{\oplus}\dot{h}_{\oplus}+h_{\otimes}\dot{h}_{\otimes})\,, \qquad (20)\\
&H_2^{13}=-H_2^{31}\\
&\quad=\frac{1}{\sqrt{-g}}g_{21}(-gg^{11}g^{33})_{,3}+\frac{1}{\sqrt{-g}}g_{22}(-gg^{12}g^{33})_{,3}\\
&\quad=-\mathrm{i}ka^2h_{\otimes}\,, \qquad (21)\\
&H_2^{23}=-H_2^{32}\\
&\quad=\frac{1}{\sqrt{-g}}g_{21}(-gg^{21}g^{33})_{,3}+\frac{1}{\sqrt{-g}}g_{22}(-gg^{22}g^{33})_{,3}\\
&\quad=\mathrm{i}ka^2\big(h_{\oplus}-h_{\oplus}^2-h_{\otimes}^2\big)\,, \qquad (22)\\
&H_3^{03}=-H_3^{30}\\
&\quad=\frac{1}{\sqrt{-g}}g_{33}(gg^{33}g^{00})_{,0}\\
&\quad=4a\dot{a}-2a\dot{a}\big(h_{\oplus}^2+h_{\otimes}^2\big)-2a^2(h_{\oplus}\dot{h}_{\oplus}+h_{\otimes}\dot{h}_{\otimes})\,, \qquad (23)
\end{aligned}$$

From (4)–(10), (13) and (14), we obtain the energy density and energy flux density as follows, respectively:

$$\begin{aligned}
&t_0^0=\frac{c^4}{16\pi G\sqrt{-g}}H_{0,\sigma}^{0\sigma}=\frac{c^4k^2}{4\pi Ga^2}\big(h_{\oplus}^2+h_{\otimes}^2\big)\,, \qquad (24)\\
&ct_0^1=cH_{0,\sigma}^{1\sigma}=ct_0^2=cH_{0,\sigma}^{2\sigma}=0\,, \qquad (25)\\
&ct_0^3=\frac{c^5}{16\pi G\sqrt{-g}}H_{0,\sigma}^{3\sigma}\\
&\quad=\frac{\mathrm{i}kc^5}{4\pi Ga^3}\big[\dot{a}\big(h_{\oplus}^2+h_{\otimes}^2\big)+a(h_{\oplus}\dot{h}_{\oplus}+h_{\otimes}\dot{h}_{\otimes})\big]\,. \qquad (26)
\end{aligned}$$

For the "monochromatic components" propagating along the x- and y-axes, we have the same expression for the energy density, (24), but $t_0^2=t_0^3=0$ and $t_0^1=t_0^3=0$, respectively. The energy flux density also has the same form, (26). Thus, the energy density of the HFRGWs is positive definite, and the energy flux densities have a reasonable physical behavior in conformal time coordinates. If we integrate the EMPT for all "the monochromatic components" of the HFRGWs, then we can find that the EMPT is homogeneous and isotropic. Riazuelo and Uzan [3] obtained an expression for the EMPT of the relic GWs in the momentum space; the average values of such expressions for the EMPT have a reasonable physical behavior. However, (4) shows that the stochastic relic GWs background contains every possible propagating direction, and because of stochastic fluctuation of the amplitudes of the HFRGWs over their bandwidth, the detection of the HFRGWs will be more difficult than that of the monochromatic plane GWs. In this case, can the HFRGWs be selected and measured? In particular, if two HFRGWs have the same amplitude and frequency, but propagate along exactly opposite directions (standing wave), will their effects be canceled and nullified? We shall show that in our EM system the EM perturbation produced by the HFRGWs, which propagate along the positive and negative directions of the symmetrical axis (the z-axis) of the GB, will be non-symmetric and the physical effect generated by the HFRGWs propagating along other directions will also be quite different, even if they satisfy the resonant condition ($\omega_e=\omega_g$), and only the HFRGW component propagating along the positive direction of the symmetrical z-axis of the GB can generate an optimal resonant response. Thus, our EM system design will be very sensitive to the propagating directions as well as the frequencies of the HFRGWs, and it may provide a HFRGW map of the celestial sphere (similar to the map of the relic microwave background provided by the Wilkinson microwave anisotropic probe or WMAP).

3 The electromagnetic resonant system: the coupling system of the fractal membranes and the Gaussian beam (GB) passing though a static magnetic field

Our EM system consists of the GB of a fundamental frequency mode [56] operating in the GHz band immersed in a static magnetic field, with a new type of fractal membranes [57–59] to focus the PPF signal along the detection axis. In order to consider a resonant response to the HFRGWs in the laboratory frame of reference, all parameters of the EM system should be values in the frame of reference. The general form of the GB of a fundamental frequency mode [56] is

$$\psi = \frac{\psi_0}{\sqrt{1+(z/f)^2}} \exp\left(-\frac{r^2}{W^2}\right) \times \exp\left\{\mathrm{i}\left[(k_e z-\omega_e t)-\tan^{-1}\frac{z}{f}+\frac{k_e r^2}{2R}+\delta\right]\right\}, \tag{27}$$

where $r^2=x^2+y^2$, $k_e=2\pi/\lambda_e$, $f=\pi W_0^2/\lambda_e$, $W=W_0[1+(z/f)^2]^{1/2}$, $R=z+f^2/z$ and ψ_0 is the amplitude of the electric (or magnetic) field of the GB, W_0 is the minimum spot radius, R is the curvature radius of the wave fronts of the GB at z, ω_e is the angular frequency, λ_e is the EM wavelength, the z-axis is the symmetrical axis of the GB, and δ is an arbitrary phase factor. For the resonant response to a HFRGW, δ is the phase difference between the GB and the resonant component of the HFRGW. Using a new approach, different from [21, 22], we choose the GB with the double transverse polarized electric modes (DTEM), and we utilize the coupling effect between the fractal membrane in the GHz band and the GB passing through a static magnetic field. Indeed, the GBs with the DTEM exhibit more realizable modes; they have been extensively discussed and applied in closed resonant cavities, open resonators and free space [56, 60–62], including the standing-wave-type and traveling-wave-type GBs. Moreover, a very important property of the EM system is that the PPF (signal) reflected or transmitted by the fractal membranes exhibits a very small decay [57–59] in transit to the detectors (high-sensitivity microwave photon flux receivers) compared with the very large decay (typical Gaussian decay rate) of the much stronger BPF. This property provides a possibility to distinguish them in some suitable regions.

If the static magnetic field pointing along the y-axis is localized in the region $-l_1 \le z \le l_2$, setting $\tilde{E}_x^{(0)}=\psi=\psi_x$ and using the condition of non-divergence, $\nabla\cdot\mathbf{E}=\frac{\partial\psi_x}{\partial x}+\frac{\partial\psi_y}{\partial y}=0$ and $\tilde{\mathbf{B}}^{(0)}=-\frac{\mathrm{i}}{\omega_e}\nabla\times\tilde{\mathbf{E}}^{(0)}$ (we use MKS units), we have

$$\begin{aligned}
&\tilde{E}_x^{(0)}=\psi=\psi_x\,,\\
&\tilde{E}_y^{(0)}=\psi_y=-\int\frac{\partial\psi_x}{\partial x}\,\mathrm{d}y=2x\left(\frac{1}{W^2}-\mathrm{i}\frac{k_e}{2R}\right)\int\psi_x\,\mathrm{d}y\,,\\
&\tilde{E}_z^{(0)}=0\,,
\end{aligned} \tag{28}$$

$$\begin{aligned}
&\tilde{B}_x^{(0)}=\frac{\mathrm{i}}{\omega_e}\frac{\partial\psi_y}{\partial z}\,,\\
&\tilde{B}_y^{(0)}=-\frac{\mathrm{i}}{\omega_e}\frac{\partial\psi_x}{\partial z}\,,\\
&\tilde{B}_z^{(0)}=\frac{\mathrm{i}}{\omega_e}\left(\frac{\partial\psi_x}{\partial y}-\frac{\partial\psi_y}{\partial x}\right),
\end{aligned} \tag{29}$$

and

$$\hat{B}^{(0)}=\begin{cases}\hat{B}_y^{(0)} & (-l_1\le z\le l_2)\,,\\ 0 & (z\le -l_1 \text{ and } z>l_2)\,,\end{cases} \tag{30}$$

where the superscript 0 denotes the background EM fields, and the notation $\tilde{}$ and $\hat{}$ stands for the time-dependent and static EM fields, respectively. For the high-frequency EM power flux (or in quantum language: photon flux), only non-vanishing average values of this with respect to time have an observable effect. From (27)–(29), one finds

$$\begin{aligned}
n_x^{(0)}&=\frac{1}{\hbar\omega_e}\left\langle\frac{1}{\mu_0}\big(\tilde{E}_y^{(0)}\tilde{B}_z^{(0)}\big)\right\rangle\\
&=\frac{1}{2\mu_0\hbar\omega_e}\,\mathrm{Re}\left\{\psi_y^*\left[\frac{\mathrm{i}}{\omega_e}\left(\frac{\partial\psi_x}{\partial y}-\frac{\partial\psi_y}{\partial x}\right)\right]\right\}\\
&=f_x^{(0)}\exp\left(-\frac{2r^2}{W^2}\right),
\end{aligned} \tag{31}$$

$$\begin{aligned}
n_y^{(0)}&=-\frac{1}{\hbar\omega_e}\left\langle\frac{1}{\mu_0}\big(\tilde{E}_x^{(0)}\tilde{B}_z^{(0)}\big)\right\rangle\\
&=\frac{1}{2\mu_0\hbar\omega_e}\,\mathrm{Re}\left\{\psi_x^*\left[\frac{\mathrm{i}}{\omega_e}\left(\frac{\partial\psi_y}{\partial x}-\frac{\partial\psi_x}{\partial y}\right)\right]\right\}\\
&=f_y^{(0)}\exp\left(-\frac{2r^2}{W^2}\right),
\end{aligned} \tag{32}$$

$$\begin{aligned}
n_z^{(0)}&=\frac{1}{\hbar\omega_e}\left\langle\frac{1}{\mu_0}\big(\tilde{E}_x^{(0)}\tilde{B}_y^{(0)}\big)-\frac{1}{\mu_0}\big(\tilde{E}_y^{(0)}\tilde{B}_x^{(0)}\big)\right\rangle\\
&=\frac{1}{2\mu_0\hbar\omega_e}\,\mathrm{Re}\left\{\psi_x^*\left[\frac{\mathrm{i}}{\omega_e}\left(\frac{\partial\psi_y}{\partial z}\right)\right]+\psi_y^*\left[\frac{\mathrm{i}}{\omega_e}\left(\frac{\partial\psi_x}{\partial z}\right)\right]\right\}\\
&=f_z^{(0)}\exp\left(-\frac{2r^2}{W^2}\right),
\end{aligned} \tag{33}$$

where $\hbar\omega_e$ is the energy of single photon, $n_x^{(0)}$, $n_y^{(0)}$ and $n_z^{(0)}$ represent the average values of the x-, y- and z-components of the BPF densities, in units of photons per second per square meter, propagating along the x-, y- and z-axes, respectively, and the angular brackets denote the average over time; $f_x^{(0)}$, $f_y^{(0)}$ and $f_z^{(0)}$ are functions of ψ_0, W_0, ω_e, r and z. Because of the non-vanishing $n_x^{(0)}$ and $n_y^{(0)}$, the GB will be asymptotically spread as $|z|$ increases (i.e., the irradiance surface of the GB spreads out in the $+z$- and $-z$-directions).

4 The EM resonant response to the HFRGWs

For the EM resonant response in the laboratory frame of reference, we should use the intervals of the laboratory

time (i.e., $c\,\mathrm{d}t = a(\eta)\,\mathrm{d}\eta$) and the laboratory frequency of the HFRGWs. In this case, (4) can be written as

$$h(\mathbf{x},t) = A(k_g)/a(t)\exp[\mathrm{i}(\mathbf{k}_g\cdot\mathbf{x}-\omega_g t)] + B(k_g)/a(t)\exp[\mathrm{i}(\mathbf{k}_g\cdot\mathbf{x}+\omega_g t)]\,, \tag{34}$$

where A/a and B/a are the stochastic values of the amplitudes of the HFRGWs in the laboratory frame of reference, k_g and ω_g are the corresponding wave vector and angular frequency in the frame of reference. Equation (34) can be seen as the approximate form of each "monochromatic polarization component" of the HFRGWs in the GHz band. In our EM system, since only the "monochromatic component" of the HFGW propagating along the positive direction of the symmetrical axis (the z-axis) of the GB generates an optimal resonant response (see Sect. 5), our attention will be focused on a circular polarized "monochromatic component" of the HFRGW in the z-direction, i.e.,

$$\begin{aligned} h_\oplus &= h_{11} = -h_{22} = A_\oplus\exp[\mathrm{i}(k_g z-\omega_g t)]\,,\\ h_\otimes &= h_{12} = h_{21} = \mathrm{i}A_\otimes\exp[\mathrm{i}(k_g z-\omega_g t)]\,, \end{aligned} \tag{35}$$

where $A_\oplus, A_\otimes \approx A(k_g)/a(t)$ (see (34)). Using the electrodynamical equations in curved spacetime,

$$\frac{1}{\sqrt{-g}}\frac{\partial}{\partial x^\nu}\big(\sqrt{-g}g^{\mu\alpha}g^{\nu\beta}F_{\alpha\beta}\big) = \mu_0 J^\mu\,, \tag{36}$$

$$\nabla_\alpha F_{\mu\nu} + \nabla_\nu F_{\alpha\mu} + \nabla_\mu F_{\nu\alpha} = 0\,, \tag{37}$$

we can describe the EM perturbation produced by the HFRGWs in the EM system, where $F_{\mu\nu}$ is the EM field tensor, and $F_{\mu\nu} = F^{(0)}_{\mu\nu} + \tilde{F}^{(1)}_{\mu\nu}$, $F^{(0)}_{\mu\nu}$ and $\tilde{F}^{(1)}_{\mu\nu}$ represent the background and first-order perturbative EM fields, respectively, in the presence of the HFRGWs. J^μ indicates the four-dimensional electric current density. For the EM response in vacuum, $J^\mu = 0$ in (36). Because of the weak field property of the HFRGWs, perturbation methods will still be valid. Using (9), (10) and (13), (36) and (37) can be reduced to

$$\begin{aligned} &\frac{\partial}{\partial x^\nu}\big[a^4 g^{\mu\alpha}g^{\nu\beta}\big(F^{(0)}_{\alpha\beta}+\tilde{F}^{(1)}_{\alpha\beta}\big)\big]\\ &\quad = \frac{\big(h_\oplus\frac{\partial h_\oplus}{\partial x_\nu} + h_\otimes\frac{\partial h_\otimes}{\partial x_\nu}\big)\big[a^4 g^{\mu\alpha}g^{\nu\beta}\big(F^{(0)}_{\alpha\beta}+\tilde{F}^{(1)}_{\alpha\beta}\big)\big]}{1-h_\oplus^2-h_\otimes^2}\,, \end{aligned} \tag{38}$$

$$\nabla_\alpha\big(F^{(0)}_{\mu\nu}+\tilde{F}^{(1)}_{\mu\nu}\big) + \nabla_\nu\big(F^{(0)}_{\alpha\mu}+\tilde{F}^{(1)}_{\alpha\mu}\big) + \nabla_\mu\big(F^{(0)}_{\nu\alpha}+\tilde{F}^{(1)}_{\nu\alpha}\big) = 0\,. \tag{39}$$

Unlike plane monochromatic GWs, the amplitudes of the relic GW in (34) are not constant, and in this case solving (38) and (39) will often be difficult. In our case, fortunately, since this is the EM response in the GHz band, and considering (35), the following equivalent relations would be valid provided $\omega_g \gg \dot{a}/a$:

$$\frac{\partial}{\partial t} \to \mp\mathrm{i}\omega_g\,, \quad \nabla \to \mathrm{i}\mathbf{k}_g\,. \tag{40}$$

In this case the process of solving (38) and (39) can be greatly simplified without excluding their essential physical features.

Introducing (9), (10), (13) and (35) into (38) and (39), considering $|h_\oplus|, |h_\otimes| \ll 1$, using the equivalent relations, (40), and neglecting high-order infinitely small quantities, the first-order perturbative EM fields generated by the direct interaction of the z-component of a certain "monochromatic wave", (35), with the static magnetic field $\hat{B}^{(0)}_y$, can be given by [14, 21, 28]

$$\begin{aligned} \tilde{E}^{(1)}_x &= \frac{\mathrm{i}}{2}A_\oplus\hat{B}^{(0)}_y k_g c(z+l_1)\exp[\mathrm{i}(k_g z-\omega_g t)] + \frac{1}{4}A_\oplus\hat{B}^{(0)}_y c\exp[\mathrm{i}(k_g z+\omega_g t)]\,,\\ \tilde{B}^{(1)}_y &= \frac{\mathrm{i}}{2}A_\oplus\hat{B}^{(0)}_y k_g(z+l_1)\exp[\mathrm{i}(k_g z-\omega_g t)] - \frac{1}{4}A_\oplus\hat{B}^{(0)}_y\exp[\mathrm{i}(k_g z+\omega_g t)]\,,\\ \tilde{E}^{(1)}_y &= -\frac{1}{2}A_\otimes\hat{B}^{(0)}_y k_g c(z+l_1)\exp[\mathrm{i}(k_g z-\omega_g t)] + \frac{\mathrm{i}}{4}A_\otimes\hat{B}^{(0)}_y c\exp[\mathrm{i}(k_g z+\omega_g t)]\,,\\ \tilde{B}^{(1)}_x &= \frac{1}{2}A_\otimes\hat{B}^{(0)}_y k_g(z+l_1)\exp[\mathrm{i}(k_g z-\omega_g t)] + \frac{\mathrm{i}}{4}A_\otimes\hat{B}^{(0)}_y\exp[\mathrm{i}(k_g z+\omega_g t)]\,, \end{aligned} \tag{41}$$

where $A_\oplus, A_\otimes \approx A(k_g)/a(t)$ (see (34)), $-l_1 \le z \le l_2$. Equation (41) shows that the first-order perturbative EM fields have a space accumulation effect ($\propto z$) in the interacting region: this is because the GWs (gravitons) and EM waves (photons) have the same propagating velocity, so that the two waves can generate an optimum coherent effect in the propagating direction [14, 28]. Such results and the calculation by Feynman perturbation techniques in [14] are self-consistent. In our EM system, we shall neglect the EM perturbation solution which describes the EM perturbation propagating along the negative direction of the z-axis, since it cannot satisfy the boundary condition $\tilde{F}^{(1)}_{\mu\nu}|_{z=-l_1} = 0$. Obviously, this is typically the inverse Gertsenshtein effect [13]. From (28)–(30) and (41), the total EM field tensors in the presence of the HFRGW can be written as

$$F_{\mu\nu} = F^{(0)}_{\mu\nu} + \tilde{F}^{(1)}_{\mu\nu} = \begin{pmatrix} 0 & \frac{1}{c}\big(\tilde{E}^{(0)}_x+\tilde{E}^{(1)}_x\big) & \frac{1}{c}\big(\tilde{E}^{(0)}_y+\tilde{E}^{(1)}_y\big) & 0\\ -\frac{1}{c}\big(\tilde{E}^{(0)}_x+\tilde{E}^{(1)}_x\big) & 0 & -\tilde{B}^{(0)}_z & \big(\hat{B}^{(0)}_y+\tilde{B}^{(0)}_y+\tilde{B}^{(1)}_y\big)\\ -\frac{1}{c}\big(\tilde{E}^{(0)}_y+\tilde{E}^{(1)}_y\big) & \tilde{B}^{(0)}_z & 0 & -\big(\tilde{B}^{(0)}_x+\tilde{B}^{(1)}_x\big)\\ 0 & -\big(\hat{B}^{(0)}_y+\tilde{B}^{(0)}_y+\tilde{B}^{(1)}_y\big) & \big(\tilde{B}^{(0)}_x+\tilde{B}^{(1)}_x\big) & 0 \end{pmatrix}. \tag{42}$$

In our exemplar EM system we have chosen the GB power of $P = 10\,\mathrm{W}$ and the static magnetic field of $\hat{B}^{(0)}_y = 3\,\mathrm{T}$; then the corresponding magnetic field amplitude of the GB is only $\tilde{B}^{(0)} \sim 10^{-5}\,\mathrm{T}$, so the ratio of $\tilde{B}^{(0)}$ and the background static magnetic field $\hat{B}^{(0)}_y$ is roughly $\tilde{B}^{(0)}/\hat{B}^{(0)}_y \sim$

10^{-5}. In this case we have neglected the perturbation EM fields produced by the directed interaction of the HFRGW with the GB.

Using the generic expression of the energy-momentum tensor of the EM fields in the GW fields,

$$T^{\mu\nu} = \frac{1}{\mu_0}\left(-F^{\mu}_{\alpha}F^{\nu\alpha} + \frac{1}{4}g^{\mu\nu}F_{\alpha\beta}F^{\alpha\beta}\right), \tag{43}$$

we can calculate the perturbation of the energy-momentum of the EM fields in the GW fields. Because of the weak field property of the HFRGWs, the energy-momentum tensor $T^{\mu\nu}$ can also be decomposed into

$$T^{\mu\nu} = \overset{(0)}{T^{\mu\nu}} + \overset{(1)}{T^{\mu\nu}} + \overset{(2)}{T^{\mu\nu}}, \tag{44}$$

where $\overset{(0)}{T^{\mu\nu}}$ is the energy-momentum tensor of the background EM fields, $\overset{(1)}{T^{\mu\nu}}$ and $\overset{(2)}{T^{\mu\nu}}$ are first- and second-order perturbations to $\overset{(0)}{T^{\mu\nu}}$ in the presence of the HFRGW. From (43) and (44), $\overset{(0)}{T^{\mu\nu}}$, $\overset{(1)}{T^{\mu\nu}}$ and $\overset{(2)}{T^{\mu\nu}}$ can be written as

$$\overset{(0)}{T^{\mu\nu}} = \frac{1}{\mu_0}\left[-F^{\mu(0)}_{\alpha}F^{\nu\alpha(0)} + \frac{1}{4}\delta^{\mu\nu}F^{(0)}_{\alpha\beta}F^{\alpha\beta(0)}\right], \tag{45}$$

$$\begin{aligned}\overset{(1)}{T^{\mu\nu}} = \frac{1}{\mu_0}\Bigg[&-\left(F^{\mu(0)}_{\alpha}\tilde{F}^{\nu\alpha(1)} + \tilde{F}^{\mu(1)}_{\alpha}F^{\nu\alpha(0)}\right)\\ &+\frac{1}{4}\delta^{\mu\nu}\left(\tilde{F}^{(1)}_{\alpha\beta}F^{\alpha\beta(0)} + F^{(0)}_{\alpha\beta}\tilde{F}^{\alpha\beta(1)}\right)\\ &-\frac{1}{4}h^{\mu\nu}F^{(0)}_{\alpha\beta}F^{\alpha\beta(0)}\Bigg],\end{aligned} \tag{46}$$

$$\begin{aligned}\overset{(2)}{T^{\mu\nu}} = \frac{1}{\mu_0}\Bigg[&-\tilde{F}^{\mu(1)}_{\alpha}\tilde{F}^{\nu\alpha(1)} + \frac{1}{4}\delta^{\mu\nu}\tilde{F}^{(1)}_{\alpha\beta}\tilde{F}^{\alpha\beta(1)}\\ &-\frac{1}{4}h^{\mu\nu}\left(F^{(0)}_{\alpha\beta}\tilde{F}^{\alpha\beta(1)} + \tilde{F}^{(1)}_{\alpha\beta}F^{\alpha\beta(0)}\right)\Bigg].\end{aligned} \tag{47}$$

Equations (41), (42), (46), and (47) show that the first-order perturbation $\tilde{F}^{(1)}_{\mu\nu}$ of the EM fields tensor contains only the first-order term of the metric h; thus $\overset{(1)}{T^{\mu\nu}}$ is proportional to the first-order terms of h, while $\overset{(2)}{T^{\mu\nu}}$ is proportional to the second-order terms of h. Because the expected amplitude of HFRGWs in the GHz band would only be $h \sim 10^{-28}$–$10^{-33}/\sqrt{\text{Hz}}$ [1, 2, 7, 8, 40, 41, 53], for non-vanishing $\overset{(0)}{T^{\mu\nu}}$, $\overset{(1)}{T^{\mu\nu}}$ and $\overset{(2)}{T^{\mu\nu}}$, we have

$$|\overset{(0)}{T^{\mu\nu}}| \gg |\overset{(1)}{T^{\mu\nu}}| \gg |\overset{(2)}{T^{\mu\nu}}|. \tag{48}$$

In this case, for the effect of the HFRGW, we are interested in $\overset{(1)}{T^{\mu\nu}}$ but not in $\overset{(0)}{T^{\mu\nu}}$ and $\overset{(2)}{T^{\mu\nu}}$. Considering the transverse and traceless (TT) gauge condition ($h^{11} = -h^{22} = h_{\oplus}$, $h^{12} = h^{21} = h_{\otimes}$, $h^{i}_{i} = 0$, $h^{01} = h^{02} = h^{03} = h^{13} = h^{23} = h^{33} = 0$), all non-vanishing components of the first-order perturbation to $T^{\mu\nu}$ generated by a "monochromatic component" propagating along the z-axis of the HFRGW can be written as

$$\begin{aligned}\overset{(1)}{T^{00}} = \frac{1}{\mu_0}\Bigg[&-\left(F^{0(0)}_{\alpha}\tilde{F}^{0\alpha(1)} + \tilde{F}^{0(1)}_{\alpha}F^{0\alpha(0)}\right)\\ &+\frac{1}{4}\left(\tilde{F}^{(1)}_{\alpha\beta}F^{\alpha\beta(0)} + F^{(0)}_{\alpha\beta}\tilde{F}^{\alpha\beta(1)}\right)\Bigg],\end{aligned} \tag{49}$$

$$\overset{(1)}{T^{01}} = -\frac{1}{\mu_0}\left(F^{0(0)}_{\alpha}\tilde{F}^{1\alpha(1)} + \tilde{F}^{0(1)}_{\alpha}F^{1\alpha(0)}\right), \tag{50}$$

$$\overset{(1)}{T^{02}} = -\frac{1}{\mu_0}\left(F^{0(0)}_{\alpha}\tilde{F}^{2\alpha(1)} + \tilde{F}^{0(1)}_{\alpha}F^{2\alpha(0)}\right), \tag{51}$$

$$\overset{(1)}{T^{03}} = -\frac{1}{\mu_0}\left(F^{0(0)}_{\alpha}\tilde{F}^{3\alpha(1)} + \tilde{F}^{0(1)}_{\alpha}F^{3\alpha(0)}\right), \tag{52}$$

$$\begin{aligned}\overset{(1)}{T^{11}} = \frac{1}{\mu_0}\Bigg[&-\left(F^{1(0)}_{\alpha}\tilde{F}^{1\alpha(1)} + \tilde{F}^{1(1)}_{\alpha}F^{1\alpha(0)}\right)\\ &+\frac{1}{4}\left(\tilde{F}^{(1)}_{\alpha\beta}F^{\alpha\beta(0)} + F^{(0)}_{\alpha\beta}\tilde{F}^{\alpha\beta(1)}\right)\\ &-\frac{1}{4}h^{11}F^{(0)}_{\alpha\beta}F^{\alpha\beta(0)}\Bigg],\end{aligned} \tag{53}$$

$$\begin{aligned}\overset{(1)}{T^{22}} = \frac{1}{\mu_0}\Bigg[&-\left(F^{2(0)}_{\alpha}\tilde{F}^{2\alpha(1)} + \tilde{F}^{2(1)}_{\alpha}F^{2\alpha(0)}\right)\\ &+\frac{1}{4}\left(\tilde{F}^{(1)}_{\alpha\beta}F^{\alpha\beta(0)} + F^{(0)}_{\alpha\beta}\tilde{F}^{\alpha\beta(1)}\right)\\ &-\frac{1}{4}h^{22}F^{(0)}_{\alpha\beta}F^{\alpha\beta(0)}\Bigg],\end{aligned} \tag{54}$$

$$\begin{aligned}\overset{(1)}{T^{33}} = \frac{1}{\mu_0}\Bigg[&-\left(F^{3(0)}_{\alpha}\tilde{F}^{3\alpha(1)} + \tilde{F}^{3(1)}_{\alpha}F^{3\alpha(0)}\right)\\ &+\frac{1}{4}\left(\tilde{F}^{(1)}_{\alpha\beta}F^{\alpha\beta(0)} + F^{(0)}_{\alpha\beta}\tilde{F}^{\alpha\beta(1)}\right)\Bigg],\end{aligned} \tag{55}$$

$$\begin{aligned}\overset{(1)}{T^{12}} = \overset{(1)}{T^{21}} = -\frac{1}{\mu_0}\Bigg[&\left(F^{1(0)}_{\alpha}\tilde{F}^{2\alpha(1)} + \tilde{F}^{1(1)}_{\alpha}F^{2\alpha(0)}\right)\\ &+\frac{1}{4}h^{12}F^{(0)}_{\alpha\beta}F^{\alpha\beta(0)}\Bigg],\end{aligned} \tag{56}$$

$$\overset{(1)}{T^{13}} = \overset{(1)}{T^{31}} = -\frac{1}{\mu_0}\left(F^{1(0)}_{\alpha}\tilde{F}^{3\alpha(1)} + \tilde{F}^{1(1)}_{\alpha}F^{3\alpha(0)}\right), \tag{57}$$

$$\overset{(1)}{T^{23}} = \overset{(1)}{T^{32}} = -\frac{1}{\mu_0}\left(F^{2(0)}_{\alpha}\tilde{F}^{3\alpha(1)} + \tilde{F}^{2(1)}_{\alpha}F^{3\alpha(0)}\right), \tag{58}$$

where $\overset{(1)}{T^{00}}$ expresses the first-order perturbation to the energy density of the EM fields, $\overset{(1)}{T^{01}}$, $\overset{(2)}{T^{02}}$ and $\overset{(3)}{T^{03}}$ indicate the first-order perturbations to the power flux densities of the EM fields in the x-, y- and z-directions, respectively, while $\overset{(1)}{T^{11}}$, $\overset{(1)}{T^{22}}$, $\overset{(1)}{T^{33}}$, $\overset{(1)}{T^{12}}$, $\overset{(1)}{T^{13}}$ and $\overset{(1)}{T^{23}}$ represent the first-order perturbations to the momentum flux density components of the EM fields.

By using (27)–(30) and (41)–(43), we can calculate the first-order PPFs produced by the HFRGW. We shall focus our attention to the 01-component $\overset{(1)}{T^{01}}$ (see (50)) of the first-order perturbation: it expresses the x-component of the power flux density (Poynting vector) of the EM

fields, i.e., the first-order perturbative power flux density generated by the coherent modulation of the preexisting x-component of the background power flux. Thus, the corresponding first-order PPF will be $c/\hbar\omega_e \overset{(1)}{T}{}^{01}$. In this case, although we do not know the value of the initial phase of "the resonant monochromatic component" of the HFRGW in the laboratory frame of reference due to its random distribution, setting the phase difference $\delta = \pi/2$ will always be possible by regulating the phase of the GB. The x-component of PPF generated by the coherent synchro-resonance ($\omega_e = \omega_g$) between the perturbative EM fields, (41) and the GB, (27)–(29), can then be expressed in the following form:

$$
\begin{aligned}
n_x^{(1)} &= \frac{c}{\hbar\omega_e}\langle \overset{(1)}{T}{}^{01}\rangle_{\omega_e=\omega_g} \\
&= -\frac{c}{\mu_0\hbar\omega_e}\left\langle F_\alpha^{0(0)}\tilde{F}^{1\alpha(1)} + \tilde{F}_\alpha^{0(1)}F^{1\alpha(0)}\right\rangle_{\omega_e=\omega_g} \\
&= \frac{1}{\hbar\omega_e}\left\langle \frac{1}{\mu_0}\tilde{E}_y^{(1)}\tilde{B}_z^{(0)}\right\rangle_{\omega_e=\omega_g} \\
&= \frac{1}{2\mu_0\hbar\omega_e}\,\mathrm{Re}\left\{\tilde{E}_y^{(1)*}\left[\frac{\mathrm{i}}{\omega_e}\left(\frac{\partial\psi_x}{\partial y} - \frac{\partial\psi_y}{\partial x})\right)\right]\right\}_{\omega_e=\omega_g} \\
&= -\frac{1}{\hbar\omega_e}\left\{\frac{A_\otimes\hat{B}_y^{(0)}\psi_0 k_g y(z+l_1)}{4\mu_0[1+(z/f)^2]^{1/2}(z+f^2/z)}\right. \\
&\quad\times\sin\left(\frac{k_g r^2}{2R} - \tan^{-1}\frac{z}{f}\right) + \frac{A_\otimes\hat{B}_y^{(0)}\psi_0 y(z+l_1)}{2\mu_0 W_0^2[1+(z/f)^2]^{3/2}} \\
&\quad\left.\times\cos\left(\frac{k_g r^2}{2R} - \tan^{-1}\frac{z}{f}\right)\right\}\exp\left(-\frac{r^2}{W^2}\right) \\
&\quad - \frac{1}{\hbar\omega_e}\left\{\left(1-\frac{4x^2}{W^2}\right)\frac{A_\otimes\hat{B}_y^{(0)}\psi_0 k_g(z+l_1)}{4\mu_0 R[1+(z/f)^2]^{1/2}}\right. \\
&\quad\times\left[F_1(y)\sin\left(\frac{k_g x^2}{2R} - \tan^{-1}\frac{z}{f}\right)\right. \\
&\quad\left.+ F_2(y)\cos\left(\frac{k_g x^2}{2R} - \tan^{-1}\frac{z}{f}\right)\right] \\
&\quad + \left[\frac{2}{W^2} + \left(\frac{k_g^2}{R^2} - \frac{4}{W^4}\right)x^2\right]\frac{A_\otimes\hat{B}_y^{(0)}\psi_0(z+l_1)}{4\mu_0[1+(z/f)^2]^{1/2}} \\
&\quad\times\left[F_1(y)\cos\left(\frac{k_g x^2}{2R} - \tan^{-1}\frac{z}{f}\right)\right. \\
&\quad\left.\left.- F_2(y)\sin\left(\frac{k_g x^2}{2R} - \tan^{-1}\frac{z}{f}\right)\right]\right\}\exp\left(-\frac{x^2}{W^2}\right),
\end{aligned}
\tag{59}
$$

where

$$
\begin{aligned}
F_1(y) &= \int \exp\left(-\frac{y^2}{W^2}\right)\cos\left(\frac{k_g y^2}{2R}\right)\mathrm{d}y\,, \\
F_2(y) &= \int \exp\left(-\frac{y^2}{W^2}\right)\sin\left(\frac{k_g y^2}{2R}\right)\mathrm{d}y
\end{aligned}
\tag{60}
$$

are the quasi-probability integrals.

It is very interesting to compare $n_x^{(0)}$, (31), and $n_x^{(1)}$, (59). From (28) and (31), we can see that $\tilde{E}_y^{(0)} = 0$ at the surface $x = 0$; thus $n_x^{(0)}|_{x=0} = 0$. Meanwhile numerical calculation shows that $n_x^{(1)}|_{x=0}$ has a maximum. This means that any photon measured by a detector (a high-sensitivity microwave receiver) from $n_x^{(1)}|_{x=0}$ will be a signal of the EM perturbation produced by the GW. Nevertheless, in the regions of $x \neq 0$, we have $n_x^{(0)} \neq 0$. At first sight $n_x^{(1)}$ will be swamped by the background $n_x^{(0)}$, so that $n_x^{(1)}$ has no observable effect in this region. However, it will be shown that $n_x^{(1)}$ and $n_x^{(0)}$ propagate along opposite directions in some local regions, and they have different rates of decay. Thus, $n_x^{(1)}$ and $n_x^{(0)}$ can be separated by special fractal membranes (see below), so that $n_x^{(1)}$ (signal), in principle, would be observable. The total PPF passing through a certain "typical receiving surface" Δs at the y–z plane will be

$$
N_x^{(1)} = \iint\limits_{\Delta s} n_x^{(1)}|_{x=0}\,\mathrm{d}y\,\mathrm{d}z\,. \tag{61}
$$

Notice that $N_x^{(1)}$ is a unique non-vanishing photon flux passing through the surface i.e., a number of photons per second. Equations (59) and (60) show that $n_x^{(1)}$ is an even function of the coordinates x; thus, $n_x^{(1)}$ has the same propagating direction in the regions of $x > 0$ and $x < 0$. At the same time, $n_x^{(1)}$ is an odd function of the coordinate y, so the propagating directions of $n_x^{(1)}$ are anti-symmetric in the regions of $y > 0$ and $y < 0$ (such a property ensured conservation of the total momentum in the coherent resonance interaction). Considering the outgoing (and imploding; i.e., they go in both directions) property of $N_x^{(0)}$ in the region $z > 0$ (and $z < 0$) (this is a typical property of the GB [56]), it can be seen that $N_x^{(1)}$ and $N_x^{(0)}$ propagate along opposite directions in the regions of the 1st ($x, y, z > 0$), 3rd ($x, y < 0$, $z > 0$), 6th ($x < 0, y > 0$, $z < 0$) and 8th ($x > 0$, $y, z < 0$) octants of the reacting region between the magnetic poles, while they have the same propagating directions in the regions of the 2nd, 4th, 5th and 7th octants (see Figs. 1–4). In our EM system example, all of the following parameters are chosen to exhibit values that can be realized in the proposed laboratory experiments; that is, they are state-of-the-art,

(1) $P = 10\,\mathrm{W}$, the power of the GB. In this case, $\psi_0 \approx 1.26\times10^3\,\mathrm{V\,m^{-1}}$ for the GB of the spot radius $W_0 = 0.05\,\mathrm{m}$.
(2) $\hat{B}_y^{(0)} = 3\,\mathrm{T}$, the strength of the background static magnetic field.
(3) $0 \le y \le W_0$, $0 \le z \le 0.3\,\mathrm{m}$, the integration region Δs (the receiving surface of the PPF) in (61), i.e., $\Delta s \approx 10^{-2}\,\mathrm{m}^2$.
(4) $l = l_2 + l_1 = 0.3$ and $6\,\mathrm{m}$, the interacting dimensions (or reacting region) between the relic GW and the static magnetic field.
(5) $\nu_e = \nu_g = 5\,\mathrm{GHz}$ ($\lambda_g = 0.06\,\mathrm{m}$); this is a typical frequency of the HFRGWs in the microwave band [1–6] and of the HFGW predicted by possible high-energy laboratory schemes [9, 10].

Figure 5 gives the result of numerical calculation for $N_x^{(1)}$. Figure 6 is a two-dimensional description of the nu-

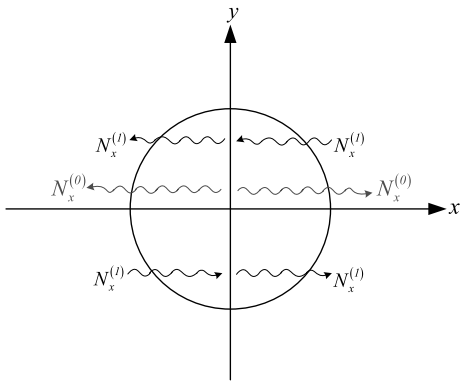

Fig. 1. $N_x^{(1)}$ (signal) and $N_x^{(0)}$ (background) in the 1st $(x, y, z > 0)$, 2nd $(x < 0,\ y, z > 0)$, 3rd $(x, y < 0,\ z > 0)$ and 4th $(x > 0,\ y < 0,\ z > 0)$ octants. $N_x^{(1)}$ and $N_x^{(0)}$ propagate along opposite directions in the regions of 1st and 3rd octants, while they have the same propagating directions in the region of 2nd and 4th octants

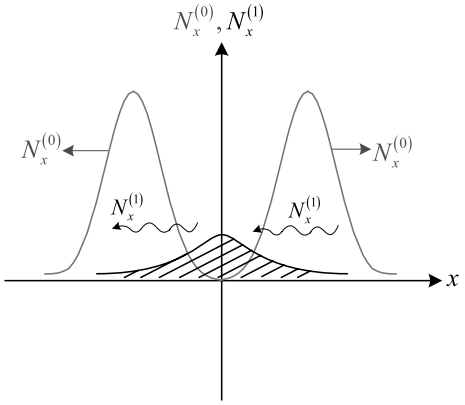

Fig. 2. Schematic diagram of strength distribution of $N_x^{(1)}$ and $N_x^{(0)}$ in the 1st and 2nd octants. We take note of $|N_x^{(0)}|_{x=0} = 0$, while $|N_x^{(1)}|_{x=0} = |N_x^{(1)}|_{\max}$, and $N_x^{(0)}$ is the "outgoing wave" to the y–z-plane

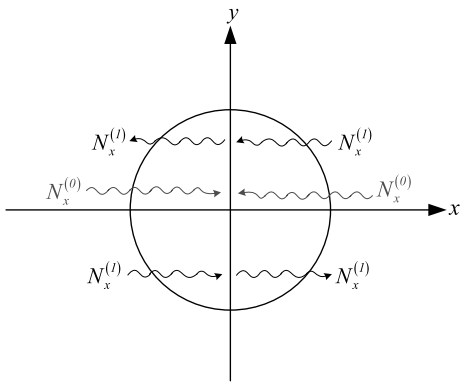

Fig. 3. $N_x^{(1)}$ and $N_x^{(0)}$ in the 5th $(x, y > 0,\ z < 0)$, 6th $(x < 0,\ y > 0,\ z < 0)$, 7th $(x, y, z < 0)$ and 8th $(x > 0, y, z > 0)$ octants. $N_x^{(1)}$ and $N_x^{(0)}$ propagate along opposite directions in the regions of the 6th and 8th octants, while they have the same propagating directions in the regions of the 5th and 7th octants

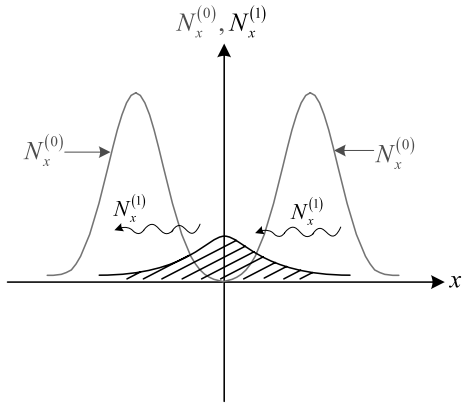

Fig. 4. Schematic diagram of strength distribution of $N_x^{(1)}$ and $N_x^{(0)}$ in the 5th and 6th octants. Also, we take note of that $|N_x^{(0)}|_{x=0} = 0$ while $|N_x^{(1)}|_{x=0} = |N_x^{(1)}|_{\max}$. Unlike Fig. 2, here $N_x^{(0)}$ is "the imploding wave" to the y–z-plane

merical calculation for the perturbative photo flux density $n_x^{(1)}$, (59). From (59)–(61), the $N_x^{(0)}$ and $N_x^{(1)}$ we obtained in a 1 Hz bandwidth are listed in Table 1.

In fact, the expected root-mean-square (r.m.s.) value $h_{\text{r.m.s.}}$ in the GHz band of the dimensionless amplitudes by the different cosmological models and parameters are quite different [1–6, 43, 52]. According to an optimistic estimation, their orders may be $h_{\text{r.m.s.}} \sim 10^{-29}$–$10^{-30}/\sqrt{\text{Hz}}$, while a conservative estimation may be only $h_{\text{r.m.s.}} \sim 10^{-34}$–$10^{-35}/\sqrt{\text{Hz}}$. References [40, 41] provide a more average estimation for the r.m.s. value $h_{\text{r.m.s.}} \sim 10^{-30}$–$10^{-32}/\sqrt{\text{Hz}}$ (see Fig. 7). Thus, in order to detect the HFRGWs in the GHz band, the minimal detectable amplitudes of the detecting systems would be

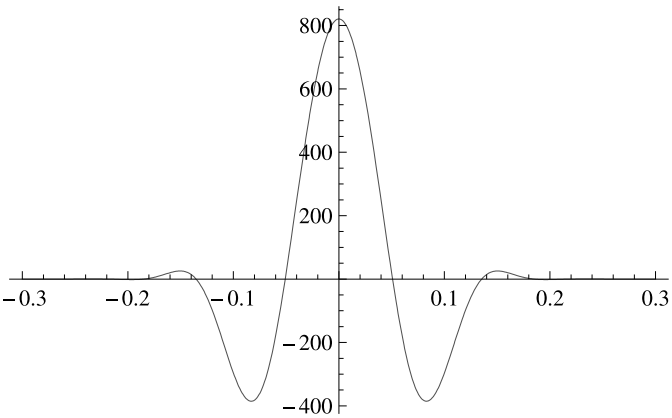

Fig. 5. The perturbative photon flux $N_x^{(1)}$ (s^{-1}) generated by the HFGW of $h_{\text{rms}} = 10^{-30}/\sqrt{\text{Hz}}$ and $\nu = 5\,\text{GHz}$, here detecting bandwidths $\Delta\nu = 1\,\text{Hz}$, $|N_x^{(1)}| = |N_x^{(1)}|_{\max} = 8.21 \times 10^2\ \text{s}^{-1}$ at $x = 0$, we take note of the background photon flux $N_x^{(0)}|_{x=0} = 0$ (see (28) and (31)); thus, $N_x^{(1)}$ would be an observable value, and $N_x^{(1)}$ and $N_x^{(0)}$ propagate along opposite directions in the first octant

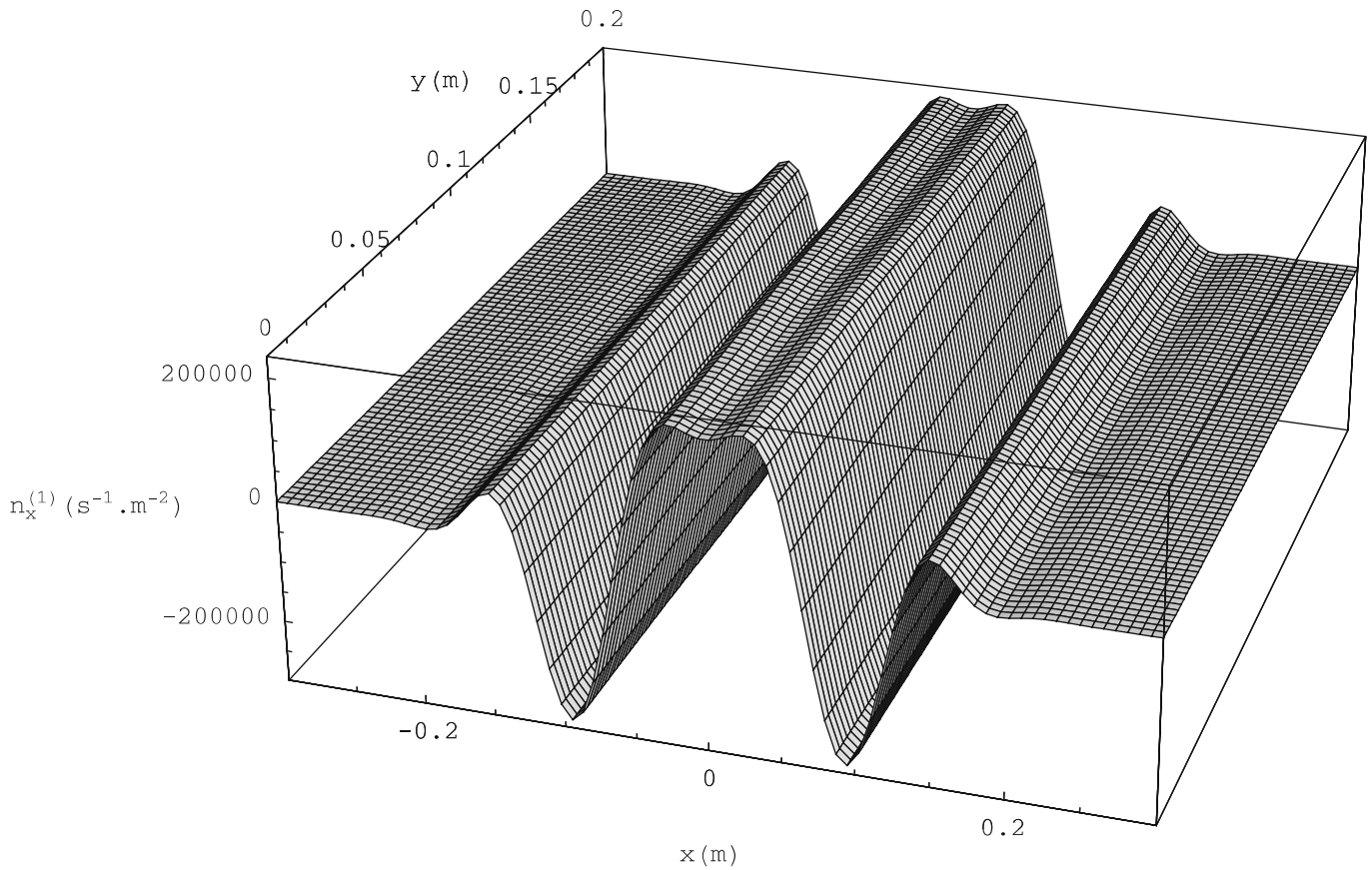

Fig. 6. Two-dimensional distribution of the perturbative photon flux density $n_x^{(1)}$ ($\mathrm{s}^{-1}\,\mathrm{m}^{-2}$) (59), where $z = l_2 = 0.3\,\mathrm{m}$, $l_1 = 5.7\,\mathrm{m}$, i.e., $z + l_1 = l_2 + l_1 = 6\,\mathrm{m}$, $0 < y < 0.2\,\mathrm{m}$, $A_{\otimes} = 10^{-30}/\sqrt{\mathrm{Hz}}$. It is shown that $|n_x^{(1)}|$ has a maximum distribution in the region of $-3.5\,\mathrm{cm} < x < 3.5\,\mathrm{cm}$

Table 1. The x-component of PPFs and relevant parameters. Here A is the root-means square value of the HFGW amplitudes, l is interacting dimension between the HFGWs and the static magnetic field, $N_x^{(0)}$ and $N_x^{(1)}$ are the x-components of BPF and PPF, respectively

A ($\mathrm{Hz}^{-\frac{1}{2}}$)	$l = l_1 + l_2$ (m)	$N_x^{(0)}$ (s^{-1})	$N_x^{(1)}$ (s^{-1})	$N_x^{(0)}$ (s^{-1})	$N_x^{(1)}$ (s^{-1})
		$x = 0\,\mathrm{cm}$		$x = 3.5\,\mathrm{cm}$	
10^{-22}	6	0	8.21×10^{10}	1.24×10^{22}	3.54×10^{10}
10^{-24}	6	0	8.21×10^{8}	1.24×10^{22}	3.54×10^{8}
10^{-26}	6	0	8.21×10^{6}	1.24×10^{22}	3.54×10^{6}
10^{-28}	6	0	8.21×10^{4}	1.24×10^{22}	3.54×10^{4}
10^{-30}	6	0	8.21×10^{2}	1.24×10^{22}	3.54×10^{2}
10^{-32}	6	0	8.21	1.24×10^{22}	3.54
10^{-34}	6	0	0	1.24×10^{22}	0

$h \sim 10^{-30}/\sqrt{\mathrm{Hz}}$ or less at least. Moreover, one often estimates the amplitudes of relic GWs by their energy spectra; this is useful because it allows us to quickly evaluate the cosmological importance of the generated field in a given frequency interval. However, as pointed out by Grishchuk [39], the primary and more universal concept is the amplitude, not the spectrum density. It is the field, not its energy density, which is directly measured by the GW detector. Therefore, we listed the PPFs under various amplitude conditions, ($h_{\mathrm{r.m.s.}} \sim 10^{-22}$–$10^{-34}/\sqrt{\mathrm{Hz}}$) in a 1 Hz bandwidth in Table 1. Of course, a possible distribution region of the amplitude magnitudes of the HFRGWs may be only $h_{\mathrm{r.m.s.}} \sim 10^{-30}$–$10^{-32}/\sqrt{\mathrm{Hz}}$; there are no HFRGWs as strong as $h_{\mathrm{r.m.s.}} \sim 10^{-22}$–$10^{-28}/\sqrt{\mathrm{Hz}}$, but the estimation of the PPFs can display a detecting ability and sensitivity of the EM sys-

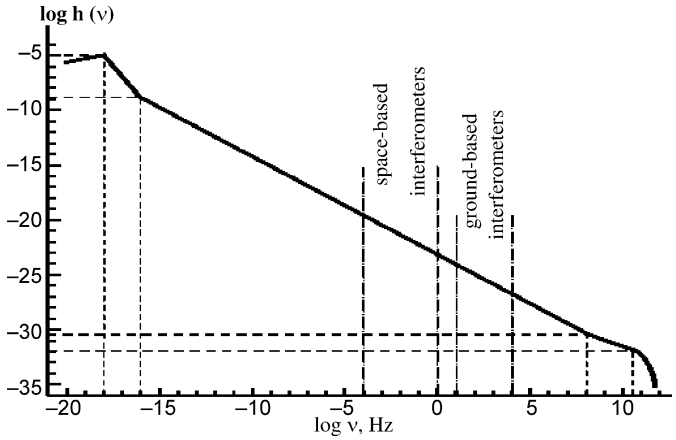

Fig. 7. Envelope of the $h_{\rm rms}(\nu)$ spectrum for a certain parameter condition. The figure is taken from [41]. The envelope shows that the r.m.s. values of the HFRGW amplitudes in the region of 10^8–10^{10} Hz would be $\sim 10^{-30}$–$10^{-32}/\sqrt{\rm Hz}$, roughly

tem in different amplitude conditions and in the frequency region.

Table 1 shows that the most interesting region would be the "typical receiving surface Δs" at the y–z plane (i.e., the plane of $x=0$), where $N_x^{(0)}|_{x=0}=0$, while $N_x^{(1)}|_{x=0}$ has a maximum (e.g., if $A=h_{\rm r.m.s.}=10^{-30}/\sqrt{\rm Hz}$ and $l=6\,{\rm m}$, then $N_x^{(1)}|_{x=0}=8.21\times10^2\,{\rm s}^{-1}$).

We emphasize that for the HFRGW and for the constant amplitude plane HFGW, even if they have the same amplitude $h_{\rm r.m.s.}=10^{-30}/\sqrt{\rm Hz}$ and the frequency $\nu=5\,{\rm GHz}$, their perturbative effects will be different. For the constant amplitude plane HFGW propagating along the symmetrical z-axis of the GB, it corresponds to a graviton flux of $N_g=3.77\times10^{16}\,{\rm s}^{-1}$ at the cross section of the waist of the GB (here the minimum spot radius of the GB is equal to 5 cm). Unlike the constant amplitude plane HFGW, due to the random property of the HFRGWs, they contain every possible propagating direction; thus, as mentioned above (Sect. 2), the propagating directions of the relic gravitons are coming near a state of isotropy. In this case, only a small fraction of the relic gravitons will pass through the cross section of the GB. However, the PPF generated by the resonant coherence modulation in our EM system is the first-order perturbation rather than the second-order perturbation of usual cavity EM response to HFGWs. Therefore, the strength of PPF is proportional to the square root $\sqrt{N_g}$ of the graviton flux (i.e., it is proportional to the amplitude of the GW, see (59)) and not the graviton flux itself N_g (i.e., the amplitude squared of the GW). In this case, numerical calculation shows that if the deviation angle from the z-axis of the propagating direction of the relic graviton flux is less than 10 degrees, then its perturbative effect and that of the graviton flux propagating along the positive direction of the z-axis (i.e., the best resonant direction, see Sect. 5) are nearly the same. Consequently, if all relic gravitons propagating along the deviation angle region ($\theta\le10^\circ$) and passing through the cross section of the GB are included, then the relic graviton flux at the cross section will be $N_g\approx2.89\times10^{14}\,{\rm s}^{-1}$ at least. This means that in this case the gap between the PPFs produced by the HFRGW and the constant amplitude HFGW will be about 1–2 orders of magnitude: this is satisfactory. Notice that then the ratio of the square roots of such graviton fluxes will be

$$\sqrt{\frac{N_{g\,\text{relic GW}}}{N_{g\,\text{plane GW}}}}=\sqrt{\frac{2.89\times10^{14}}{3.77\times10^{16}}}\approx8.76\times10^{-2}. \qquad (62)$$

From (27)–(29), (41) and (51), we can calculate the 02-component $\overset{(1)}{T}{}^{02}$ of the first-order perturbation, and the corresponding PPF will be $c/\hbar\omega_e\overset{(1)}{T}{}^{02}$, it expresses the first-order PPF density $n_y^{(1)}$ propagating along the y-direction. By using similar means, we get $n_y^{(1)}$ as follows:

$$\begin{aligned}
n_y^{(1)} &= \frac{c}{\hbar\omega_e}\langle\overset{(1)}{T}{}^{02}\rangle_{\omega_e=\omega_g}\\
&= -\frac{c}{\mu_0\hbar\omega_e}\left\langle F_\alpha^{0(0)}\tilde F^{2\alpha(1)}+\tilde F_\alpha^{0(1)}F^{2\alpha(0)}\right\rangle_{\omega_e=\omega_g}\\
&= -\frac{1}{\hbar\omega_e}\left\langle\frac{1}{\mu_0}\tilde E_x^{(1)}\tilde B_z^{(0)}\right\rangle_{\omega_e=\omega_g}\\
&= -\frac{1}{2\mu_0\hbar\omega_e}\,{\rm Re}\left\{\tilde E_x^{(1)*}\left(\frac{\partial\psi_x}{\partial y}-\frac{\partial\psi_y}{\partial x}\right)\right\}_{\omega_e=\omega_g}\\
&= \frac{1}{\hbar\omega_e}\left\{\frac{A_\oplus\hat B_y^{(0)}\psi_0k_gy(z+l_1)}{4\mu_0[1+z/f]^{\frac12}(z+f^2/z)}\right.\\
&\quad\times\cos\left(\frac{k_gr^2}{2R}-\tan^{-1}\frac{z}{f}\right)-\frac{A_\oplus\hat B_y^{(0)}\psi_0y(z+l_1)}{2\mu_0W_0^2[1+(z/f)^2]^{\frac32}}\\
&\quad\left.\times\sin\left(\frac{k_gr^2}{2R}-\tan^{-1}\frac{z}{f}\right)\right\}\exp\left(-\frac{r^2}{W^2}\right)\\
&\quad+\frac{1}{\hbar\omega_e}\left\{\left(1-\frac{4x^2}{W^2}\right)\frac{A_\oplus\hat B_y^{(0)}k_g(z+l_1)}{4\mu_0R[1+(z/f)^2]^{\frac12}}\right.\\
&\quad\times\left[F_1(y)\cos\left(\frac{k_gx^2}{2R}-\tan^{-1}\frac{z}{f}\right)\right.\\
&\quad\left.-F_2(y)\sin\left(\frac{k_gx^2}{2R}-\tan^{-1}\frac{z}{f}\right)\right]\\
&\quad-\left[\frac{2}{W^2}+\left(\frac{k_g^2}{R^2}-\frac{4}{W^4}\right)x^2\right]\frac{A_\oplus\hat B_y^{(0)}\psi_0(z+l_1)}{4\mu_0[1+(z/f)^2]^{\frac12}}\\
&\quad\times\left[F_1(y)\sin\left(\frac{k_gx^2}{2R}-\tan^{-1}\frac{z}{f}\right)\right.\\
&\quad\left.\left.+F_2(y)\cos\left(\frac{k_gx^2}{2R}-\tan^{-1}\frac{z}{f}\right)\right]\right\}\exp\left(-\frac{x^2}{W^2}\right).
\end{aligned} \qquad (63)$$

By comparing with (59) and (63), we can see that, first, $n_y^{(1)}$ is also an even function of the coordinates x and an odd function of the coordinates y. Thus, $n_y^{(1)}$ has the same propagating direction in the regions of $x>0$ and $x<0$, and $n_y^{(1)}$ has an opposite propagating direction in the regions of $y>0$ and $y<0$. However, unlike property of $n_x^{(1)}|_{x=0}=n_{x\,\max}^{(1)}$, $n_y^{(0)}|_{y=0}=0$ and we also have $n_y^{(1)}|_{y=0}=0$. There-

fore, $n_y^{(1)}$ and $n_y^{(0)}$ have very similar distribution and behavior. In other words, in almost all regions, $n_y^{(1)}$ will be swamped by the background $n_y^{(0)}$, i.e., $n_y^{(1)}$ has no observable effect.

Second, in our case, $n_x^{(1)}$ depends only on the state of the $\otimes$ polarization of the HFRGW and it is independent of the state of the $\oplus$ polarization of the HFRGW (see (59)), while $n_y^{(1)}$ depends only on the state of the $\oplus$ polarization state and is independent of the state of the $\otimes$ polarization (see (63)). Thus, the state of polarization displayable in the EM system will be only the $\otimes$ polarization component of the HFRGW rather than the $\oplus$ polarization component.

The quantum picture of the above-mentioned process can be described as the resonant interaction of the photons with the gravitons in a background of virtual photons (the static magnetic field) as a catalyst [14, 63], i.e., the interaction involving elastic scattering of the photons by the gravitons in the background of virtual photons (in the reacting region between the magnet poles), which can greatly increase the interaction cross section between the photons and the gravitons. In other words, the interaction may effectively change the physical behavior (e.g., propagating direction, distribution, polarization, and phase) of the partial photons in the local regions, and it does not require resonant conversion of the gravitons to the photons; the latter corresponds to an extremely small conversion rate [11]. Consequently, even if the net increase of the photon number (the EM energy) of the entire EM system approaches zero, then one still might find an observable effect. In this case the requirements of relative parameters can be greatly relaxed, such properties may be very useful in order to detect the very weak signal of the HFRGWs. In the case of astrophysical phenomena, an analogous example is deflection of light (an EM wave beam) in a gravitational field, which causes the deflection of the propagating direction of the light ray, and although there is no any change of the photon number, there is an observable effect. Of course, in this process the interacting gravitational fields are static (e.g., the gravitational field of the sun). Thus, there is no the frequency resonant effect between the GWs and the EM waves and the space accumulation effect caused by the coherent interaction of the two kinds of waves in the propagating direction, but huge celestial gravitational fields compensate for such a shortcoming. In our system the change of the propagating directions and distribution of the partial photons in the local regions is caused by the GW, while the strong background static magnetic field provides a catalyst to enhance the resonant effect between the EM wave (the photon flux) and the GW (gravitons), whose coupling compensates in part for the weakness of the HFRGWs.

5 The selection of the perturbative photon fluxes

Because of the randomness property of the relic GWs, detection of the relic GWs will be more difficult than that of the constant amplitude plane GWs. However, we shall show that only the relic GW component propagating along the positive direction of the z-axis can generate an optimal resonant response. It is true that for the relic GW components propagating along the x-, y-axes and the negative direction of the z-axis, even if $\omega_g = \omega_e$, the PPFs produced by them will be much less than that generated by the relic GW component propagating along the positive direction of the z-axis. Thus the perturbations produced by the relic GW components propagating along the different directions cannot be counteracted. In Fig. 8 we draw the symmetrical axis (the z-axis) of the Gaussian beam and the propagating directions k_g of the arbitrary component of the relic GWs.

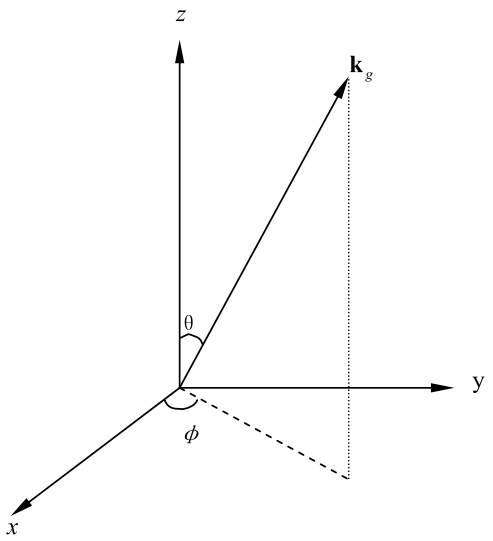

Fig. 8. The z-axis is the symmetrical axis of the Gaussian beam, k_g represents the propagating direction of the arbitrary component of the relic GW

In order to compare the PPFs generated by the different components of the HFRGW, we shall discuss the perturbations caused by the HFRGW's components propagating along some typical directions.

5.1 The PPFs generated by the HFRGW components propagating along different directions

Here we assume $A = h_{\mathrm{r.m.s.}} = 10^{-30}/\sqrt{\mathrm{Hz}}$, $\nu_e = \nu_g = 5\,\mathrm{GHz}$; the detecting bandwidth is 1 Hz.

(a) $\theta = 0$, i.e., the HFRGW component propagates along the positive direction of the z-axis. As has been calculated, the PPF generated by the component may reach up to $8.21 \times 10^2\,\mathrm{s}^{-1}$ in a surface of $10^{-2}\,\mathrm{m}^2$ area (see Table 1).

(b) $\theta = \pi$, i.e., the HFRGW component propagates along the negative direction of the z-axis.

By using similar means, one finds

$$n_x^{(1)} = -\frac{1}{\hbar\omega_e}\left\{\frac{A_{\otimes}\hat{B}_y^{(0)}\psi_0 k_g y(l_2 - z)}{4\mu_0[1+(z/f)^2]^{1/2}(z+f^2/z)} \times \sin\left(2k_g z + \frac{k_g r^2}{2R} - \tan^{-1}\frac{z}{f}\right)\right.$$

$$
\begin{aligned}
&+\frac{A_{\otimes}\hat{B}_y^{(0)}\psi_0 y(l_2-z)}{2\mu_0 W_0^2[1+(z/f)^2]^{3/2}}\\
&\times\cos\left(2k_gz+\frac{k_gr^2}{2R}-\tan^{-1}\frac{z}{f}\right)\Bigg\}\exp\left(-\frac{r^2}{W^2}\right)\\
&-\frac{1}{\hbar\omega_e}\Bigg\{\left(1-\frac{4x^2}{W^2}\right)\frac{A_{\otimes}\hat{B}_y^{(0)}\psi_0 k_g(l_2-z)}{4\mu_0R[1+(z/f)^2]^{1/2}}\\
&\times\left[F_1(y)\sin\left(2k_gz+\frac{k_gx^2}{2R}-\tan^{-1}\frac{z}{f}\right)\right.\\
&\left.+F_2(y)\cos\left(2k_gz+\frac{k_gx^2}{2R}-\tan^{-1}\frac{z}{f}\right)\right]\\
&+\left[\frac{2}{W^2}+\left(\frac{k_g^2}{R^2}-\frac{1}{W^4}\right)x^2\right]\frac{A_{\otimes}\hat{B}_y^{(0)}\psi_0(l_2-z)}{4\mu_0[1+(z/f)^2]^{1/2}}\\
&\times\left[F_1(y)\cos\left(2k_gz+\frac{k_gx^2}{2R}-\tan^{-1}\frac{z}{f}\right)\right.\\
&\left.-F_2(y)\sin\left(2k_gz+\frac{k_gx^2}{2R}-\tan^{-1}\frac{z}{f}\right)\right]\Bigg\}\\
&\times\exp\left(-\frac{x^2}{W^2}\right). \qquad (64)
\end{aligned}
$$

Different from (59), each and every term in (64) contains an oscillating factor $2k_gz$. We emphasize that $2k_gz\approx 209z$ for the high-frequency relic GW of $\nu_g=5GHz$, the factor $2k_gz$ will play a major role in the region of the effective coherent resonance. In other words, the sign of $n_x^{(1)}$ will oscillate quickly and quasi-periodically change as the coordinate z in the region increases. Thus the total effective PPF passing through a certain "typical receiving surface" will be much less than that generated by the relic GW component propagating along the positive direction of the z-axis (see (59) and Table 2).

(c) $\theta=\pi/2$, $\phi=0$, i.e., the propagating direction of the relic GW component is not only perpendicular to the symmetrical z-axis of the GB, but also perpendicular to the static magnetic field $\hat{B}_y^{(0)}$ directed along the y-axis, so that it is along the x-axis. Here we assume that the dimension of the x-direction of $\hat{B}_y^{(0)}$ is localized in the region $-l_3\le x\le l_4$. Utilizing similar means, the first-order perturbative EM fields generated by the direct interaction of the relic GW with the static magnetic field can be given by

$$
\begin{aligned}
\tilde{E}_y^{(1)}&=\frac{\mathrm{i}}{2}A_{\oplus}\hat{B}_y^{(0)}k_gc(x+l_3)\exp[\mathrm{i}(k_gx-\omega_gt)]\\
&\quad+\frac{1}{4}A_{\oplus}\hat{B}_y^{(0)}c\exp[\mathrm{i}(k_gx+\omega_gt)]\,,\\
\tilde{B}_z^{(1)}&=\frac{\mathrm{i}}{2}A_{\oplus}\hat{B}_y^{(0)}k_g(x+l_3)\exp[\mathrm{i}(k_gx-\omega_gt)]\\
&\quad-\frac{1}{4}A_{\oplus}\hat{B}_y^{(0)}\exp[\mathrm{i}(k_gx+\omega_gt)]\,,\\
\tilde{E}_z^{(1)}&=-\frac{1}{2}A_{\otimes}\hat{B}_y^{(0)}k_gc(x+l_3)\exp[\mathrm{i}(k_gx-\omega_gt)]\\
&\quad+\frac{\mathrm{i}}{4}A_{\otimes}\hat{B}_y^{(0)}c\exp[\mathrm{i}(k_gx+\omega_gt)]\,,\\
\tilde{B}_y^{(1)}&=\frac{1}{2}A_{\otimes}\hat{B}_y^{(0)}k_g(x+l_3)\exp[\mathrm{i}(k_gx-\omega_gt)]\\
&\quad+\frac{\mathrm{i}}{4}A_{\otimes}\hat{B}_y^{(0)}\exp[\mathrm{i}(k_gx+\omega_gt)] \qquad (65)\\
&\qquad\qquad(-l_3\le x\le l_4)\,.
\end{aligned}
$$

In this case, the coherent synchro-resonance ($\omega_e=\omega_g$) between the perturbative fields, (65), and the GB can be expressed as the following PPF density, i.e.,

$$
\begin{aligned}
n_x^{(1)}&=\frac{1}{\mu_0\hbar\omega_e}\left[\langle\tilde{E}_y^{(1)}\tilde{B}_z^{(0)}\rangle+\langle\tilde{E}_y^{(0)}\tilde{B}_z^{(1)}\rangle-\langle\tilde{E}_z^{(1)}\tilde{B}_y^{(0)}\rangle\right]_{\omega_e=\omega_g}\\
&=\frac{1}{2\mu_0\hbar\omega_e}\,\mathrm{Re}\left\{\tilde{E}_y^{(1)*}\left[\frac{\mathrm{i}}{\omega_e}\left(\frac{\partial\psi_x}{\partial y}-\frac{\partial\psi_y}{\partial x}\right)\right]+\psi_y^*\tilde{B}_z^{(1)}\right.\\
&\qquad\left.+\tilde{E}_z^{(1)*}\left(\frac{\mathrm{i}}{\omega_e}\frac{\partial\psi_x}{\partial z}\right)\right\}_{\omega_e=\omega_g}, \qquad (66)
\end{aligned}
$$

where $\tilde{B}_y^{(0)}$ and $\tilde{B}_z^{(0)}$ are the y- and z-components of the magnetic filed of the GB, respectively, and the angular brackets denote the average over time. Notice that we choose the GB of the transverse electric modes, so $\tilde{E}_z^{(0)}=0$. By using the same method, we can calculate $n_x^{(1)}$, (65). For example, the first term in (66) can be written as

$$
\begin{aligned}
&\frac{1}{2\mu_0\hbar\omega_e}\,\mathrm{Re}\left\{\tilde{E}_y^{(1)*}\left[\frac{\mathrm{i}}{\omega_e}\left(\frac{\partial\psi_x}{\partial y}-\frac{\partial\psi_y}{\partial x}\right)\right]\right\}_{\omega_e=\omega_g}\\
&=-\frac{1}{\hbar\omega_e}\Bigg\{\frac{A_{\oplus}\hat{B}_y^{(0)}\psi_0k_gy(x+l_3)}{4\mu_0[1+(z/f)^2]^{1/2}(z+f^2/z)}\\
&\times\sin\left[k_g(x-z)+\frac{k_gr^2}{2R}-\tan^{-1}\frac{z}{f}\right]\\
&+\frac{A_{\oplus}\hat{B}_y^{(0)}\psi_0y(x+l_3)}{2\mu_0W_0^2[1+(z/f)^2]^{3/2}}\\
&\times\cos\left[k_g(x-z)+\frac{k_gr^2}{2R}-\tan^{-1}\frac{z}{f}\right]\Bigg\}\exp\left(-\frac{r^2}{W^2}\right)\\
&-\frac{1}{\hbar\omega_e}\Bigg\{\left(1-\frac{4x^2}{W^2}\right)\frac{A_{\oplus}\hat{B}_y^{(0)}\psi_0k_gy(x+l_3)}{4\mu_0R[1+(z/f)^2]^{1/2}}\\
&\times\left[F_1(y)\sin\left(k_g(x-z)+\frac{k_gx^2}{2R}-\tan^{-1}\frac{z}{f}\right)\right]\\
&+F_2(y)\cos\left(k_g(x-z)+\frac{k_gx^2}{2R}-\tan^{-1}\frac{z}{f}\right)\\
&+\left[\frac{2}{W^2}+\left(\frac{k_g^2}{R^2}-\frac{1}{W^4}\right)x^2\right]\frac{A_{\oplus}\hat{B}_y^{(0)}\psi_0y(x+l_3)}{4\mu_0[1+(z/f)^2]^{1/2}}\\
&\times\left[F_1(y)\cos\left(k_g(x-z)+\frac{k_gx^2}{2R}-\tan^{-1}\frac{z}{f}\right)\right.
\end{aligned}
$$

Table 2. The PPFs generated by the resonant HFGW components propagating along the different directions; here $\hat{B}^{(0)}=3\,\mathrm{T}$, $A_{\otimes},A_{\oplus}\sim 10^{-30}/\sqrt{\mathrm{Hz}}$, $\nu_g=5\,\mathrm{GHz}$, $l_2+l_1=6\,\mathrm{m}$

Propagating directions of the resonant components of the relic HFGWs	$N_x^{(1)}$ (s^{-1})
z	8.21×10^2
$-z$	2.04×10
x	4.07×10^{-1}
y	0

$$- F_2(y)\sin\left(k_g(x-z)+\frac{k_g x^2}{2R}-\tan^{-1}\frac{z}{f}\right)\Bigg]\Bigg\}$$
$$\times\exp\left(-\frac{x^2}{W^2}\right) \qquad (67)$$
$$(-l_3 < x < l_4)\,.$$

It can be shown that the calculation for the second and third terms in (66) is quite similar to the first term, and they have the same orders of magnitude; we shall not repeat it here. Notice that unlike $n_x^{(1)}$ produced by the relic GW component propagating along the positive direction of the z-axis, the phase functions in (67) contain the oscillating factor $k_g(x-z)$, and because it is always possible to choose $l_2+l_1 \gg l_4+l_3$, i.e., the dimension of the z-direction of $\hat{B}_y^{(0)}$ is much larger than its x-direction dimension. Thus, the PPF expressed by (59) will be much larger than that represented by (66) (see Table 2).

(d) $\theta=\pi/2$, $\phi=\pi/2$, i.e., the relic GW component propagates along the y-axis, which is parallel to the static magnetic field $\hat{B}_y^{(0)}$.

According to the Einstein–Maxwell equations of the weak field, the perturbation of the GW to the static magnetic field vanishes [14, 28], i.e.,

$$n_x^{(1)}=0\,. \qquad (68)$$

It is very interesting to compare $n_x^{(1)}$ in (59), (64), (67) and (68), as it is shown that although they all represent PPFs propagating along the x-axis, their physical behaviors are quite different. In the case of $\theta=\phi=\pi/2$, $n_x^{(1)}=0$, (68); when $\theta=\pi$ and $\theta=\pi/2$, $\phi=0$, the PPFs contain the oscillating factors $2k_g z$ and $k_g(x-z)$, respectively (see (64) and (67)). Only under the condition $\theta=0$ does the PPF, (59), not contain any oscillating factor, but only a slow variation function in the z-direction. This means that $n_x^{(1)}$ produced by the relic GW component propagating along the positive direction of the z-axis has the best space accumulation effect (see Table 2). Thus, as previously mentioned, our EM system would be very sensitive to the propagating directions of the relic GWs. In other words the EM system has a strong selection capability to the resonant components from the stochastic relic GW background. Therefore, if the real relic GW background has a small deviation to the isotropy of space, then it should be possible to provide an HFRGW map of the celestial sphere by changing the direction of the symmetrical axis of the GB, or alternatively by the utilization of multiple EM detectors.

5.2 The separation of the PPFs (signal) from the BPFs

In recent years, new types of fractal membranes have successfully been developed [57–59]. Firstly, these fractal membranes can provide nearly total reflection for the EM waves (photon flux) with certain frequencies in the GHz band; at the same time, they can provide a nearly total transmission for the photon fluxes with other frequencies in the GHz band (the fractal-membrane pattern can be "significantly sub-wavelength in all dimensions" [57]). Secondly, the photon fluxes reflected and transmitted by the fractal membranes can keep their strength invariant within the distance of 1 meter from the fractal-membrane's surface, especially if the fractal-membrane reflectors are back-to-back very shallow (or segmented) paraboloid mirrors that focus the PPF on the detectors situated out along opposite ends of the x-axis. In this case the diffracted focus spot at each detector exhibits a radius of $\lambda_g/\pi = 6\,\mathrm{cm}/\pi \sim 1.91\,\mathrm{cm}$ (area of $\sim 10^{-4}\,\mathrm{m}^2$) [9, 10]. Thirdly, such frequencies can be regulated in the GHz band. Since $N_x^{(1)}$ (signal) and $N_x^{(0)}$ (background) propagate along the negative and positive directions of the x-axis in the first octant (the region of $x, y, z > 0$), respectively, i.e., $N_x^{(1)}$ propagates along the direction toward the fractal membrane, while $N_x^{(0)}$ propagates along the direction away from the fractal membrane (see Fig. 9). Using the reflecting fractal membranes with their plane or paraboloid faces normal to the x-axis, it will reflect only $N_x^{(1)}$ and not $N_x^{(0)}$. Once $N_x^{(1)}$ is reflected (defined as $N_x^{(1)'}$) it will have the same propagation direction as $N_x^{(0)}$. However, after $N_x^{(1)}$ is reflected, it can keep its strength invariant within 1 meter distance from the fractal membrane [57, 58], while $N_x^{(0)}$ decays by the typical Gaussian decay rate $\exp\left(-\frac{2r^2}{W^2}\right)$ (see (31)) to each side of the GB (x- and y-directed), the ratio $N_x^{(1)'}/N_x^{(0)}$ (the signal-to-background noise ratio in the x-direction) would be larger than 1 in the whole region of $0.35\,\mathrm{m} \le x \le 1\,\mathrm{m}$ (see Table 3; x is the distance from the detectors to the frac-

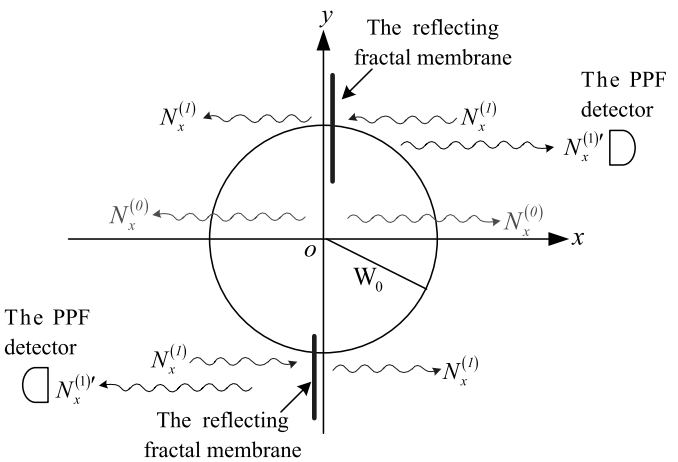

Fig. 9. $N_x^{(0)}$, $N_x^{(1)}$ and $N_x^{(1)'}$ in the 1st and 3rd octants. After $N_x^{(1)}$ is reflected by the fractal membrane, (e.g., $N_x^{(1)'}$ in the 1st and 3rd octants), $N_x^{(1)'}$ and $N_x^{(0)}$ will have the same propagating direction. However, $N_x^{(1)'}$ can keep its strength invariant within 1 m to the membrane (see, e.g., [57, 58]), while $N_x^{(0)}$ decays as the typical off-axis (radial distance r) Gaussian decay rate $\exp(-2r^2/W^2)$ (see (31)) and attenuated further by superconducting baffles; then the ratio $N_x^{(1)'}/N_x^{(0)}$ would be larger than 1 in the whole region of $0.35\,\mathrm{m} < x < 1\,\mathrm{m}$, although $N_x^{(0)} \gg N_x^{(1)'}$ in the region of $0 < x < 0.35\,\mathrm{m}$

tal membranes). Table 3 shows that the BPF $N_x^{(0)}$ is much larger than the PPF $N_x^{(1)'}$ in the region $0 < x < 35\,\mathrm{cm}$, while the $N_x^{(0)}$ and $N_x^{(1)'}$ have the same order of magnitude at $x = 35.09\,\mathrm{cm}$, and $N_x^{(1)'}$ would be larger than $N_x^{(0)}$ in the region of $x > 35\,\mathrm{cm}$. In other words, in this region the signal-to-background noise ratio $N_x^{(1)'}/N_x^{(0)}$ in the x-direction might gain up to a comparable order of magnitude. It appears to be better to use the transmitting fractal membranes, because the PPF transmitted by the fractal membrane can also keep its strength invariant within 1 meter to the membrane, and the PPF does not change its propagating direction. In this case, the PPF detectors in 1st and 3rd octants in Fig. 9 should be replaced by the detectors in 2nd and 4th octants in Fig. 10.

In fact, the circular polarized "monochromatic component", (35), is often called the right-handed circular polarization, while a left-handed circular polarized component has following form:

$$h_\oplus = h_{11} = -h_{22} = A_\oplus \exp[\mathrm{i}(k_g z - \omega_g t)]\,,$$
$$h_\otimes = h_{12} = h_{21} = -\mathrm{i}A_\otimes \exp[\mathrm{i}(k_g z - \omega_g t)]\,, \qquad (69)$$

where $A_\oplus, A_\otimes \approx A(k_g)/a(t)$. In our EM system, according to (35), (38), (39) and (69), the propagating direction of $N_x^{(1)}$ depends on the choice of the circular polarization. Thus, if the interacting "monochromatic component" is only the left-handed circular polarized state, (69), then the propagating direction of $N_x^{(1)}$ will be opposite to that generated by the right-handed circularly polarized component, (35), and then $N_x^{(1)}$ and $N_x^{(0)}$ propagate along opposite directions in the regions of the 2nd, 4th, 5th and 7th octants, while they have the same propagating direction in the regions of the 1st, 3rd, 6th and 8th octants. In such a case, the distinguishable PPF from the BPF would be $N_x^{(1)}$ in the regions of the 2nd and 4th octants but not in the regions of the 1st and 3rd octants.

If both circular polarizations exist at the same time (in this case the two polarized states often have a certain phase difference; a more detailed investigation of the issues will be done elsewhere), then the PPFs (here we defined them as $N_{x\,\mathrm{I}}^{(1)}$ and $N_{x\,\mathrm{II}}^{(1)}$, respectively) generated by the right- and left-handed polarized circular components will propagate along opposite directions in every octant. One of them propagates along the positive direction in the x-axis, and another one in the negative direction in the x-axis. However, because the effects of the fractal membranes to $N_{x\,\mathrm{I}}^{(1)}$ and $N_{x\,\mathrm{II}}^{(1)}$ are quite different, one kind of the two PPFs ($N_{x\,\mathrm{I}}^{(1)}$ or $N_{x\,\mathrm{II}}^{(1)}$) could be distinguished from the BPF.

For example, in the first octant (the region of $x, y, z > 0$) $N_{x\,\mathrm{I}}^{(1)}$ and $N_{x\,\mathrm{II}}^{(1)}$ propagate along the negative and positive directions of the x-axis, respectively. This means that $N_{x\,\mathrm{I}}^{(1)}$ propagates along the direction toward the fractal membrane, while $N_{x\,\mathrm{II}}^{(1)}$ and $N_x^{(0)}$ propagate along the direction away from the fractal membrane (see also Figs. 1, 9

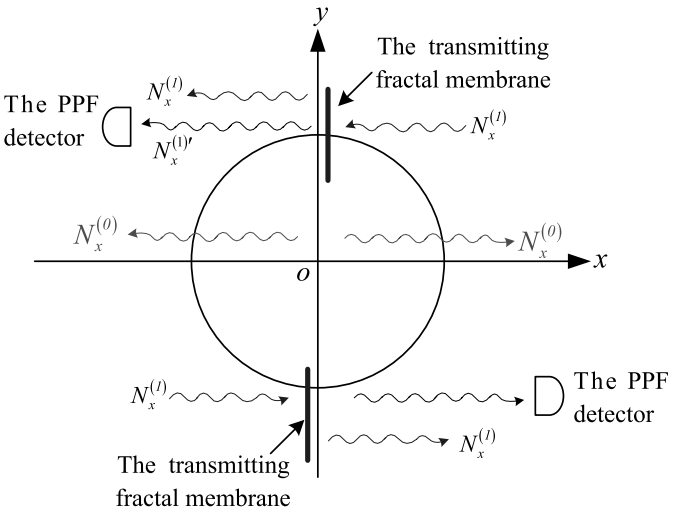

Fig. 10. $N_x^{(0)}$, $N_x^{(1)}$ and $N_x^{(1)'}$ in the 2nd and 4th octants. Unlike Fig. 9, here $N_x^{(1)'}$ is the PPF transmitted by the transmitting fractal membrane; then the PPF detectors should be put in the 2nd and 4th octants

Table 3. Comparison of the PPF reflected or transmitted by the fractal membrane and the BPF in the x-direction; here $\hat{B}^{(0)} = 3\,\mathrm{T}$, $h_{\mathrm{rms}} \sim 10^{-30}/\sqrt{\mathrm{Hz}}$, $\nu_g = 5\,\mathrm{GHz}$, $l_2 + l_1 = 6\,\mathrm{m}$ and the detecting bandwidth $\Delta\nu = 1\,\mathrm{Hz}$. The PPF $N_x^{(1)}$ reflected or transmitted (defined as $N_x^{(1)'}$) by the fractal membrane can keep its strength invariant nearly within 1 meter distance from the membrane [57–59] (or even more, attenuated by superconductor baffles along the x-axis). Even if according to the most conservative estimation to the fractal membranes [69], the photon flux reflected or transmitted by the fractal membranes can keep ninety percent of its strength at the position of 1 meter distance from the fractal membranes. Here our comparison is just from this conservative estimation. Thus, $N_x^{(1)'}$ and $N_x^{(0)}$ would be of a comparable order of magnitude in the region $35\,\mathrm{cm} < x < 37\,\mathrm{cm}$ (over a diffraction-limited spot area of $\sim 3 \times 10^{-4}\,\mathrm{m}^2$)

Distance to the fractal membrane (cm)	0	3.50	32.59	35.09	37.00
$N_x^{(0)}$ (s^{-1})	0	1.24×10^{22}	6.73×10^{5}	8.20×10^{2}	3.50
$N_x^{(1)'}$ (s^{-1})	8.21×10^{2}	8.18×10^{2}	7.94×10^{2}	7.92×10^{2}	7.90×10^{2}

and 10). In this case the PPF reflected (or transmitted) by the fractal membrane will be only $N^{(1)}_{x\,\mathrm{I}}$ but not $N^{(1)}_{x\,\mathrm{II}}$ and $N^{(0)}_{x}$. Once $N^{(1)}_{x\,\mathrm{I}}$ is reflected (or transmitted) by the fractal membrane, it will keep its strength invariant within 1 m distance from the fractal membrane [57, 58], while $N^{(0)}_{x}$ decays as the typical Gaussian decay rate $\exp\left(-\frac{2r^2}{W^2}\right)$, $N^{(1)}_{x\,\mathrm{II}}$ decay as the $\exp(-\frac{x^2}{W^2})$ (see also (59)). Therefore, the ratio $N^{(1)}_{x\,\mathrm{I}}/N^{(0)}_{x}$ would have a comparable order of magnitude in the distance of $35\,\mathrm{cm} < x < 37\,\mathrm{cm}$ from the fractal membrane (see also Table 3). In this case, in principle, $N^{(1)}_{x\,\mathrm{I}}$ can still be distinguished from $N^{(0)}_{x}$, while the other one of the PPFs $N^{(1)}_{x\,\mathrm{II}}$ will be swamped by $N^{(0)}_{x}$ due to the same propagating direction and a similar way of decaying. There is a similar property in the second octant (the region of $x < 0$, $y, z > 0$); the unique difference is that where $N^{(1)}_{x\,\mathrm{II}}$ and $N^{(0)}_{x}$ propagate along the opposite directions, $N^{(1)}_{x\,\mathrm{I}}$ and $N^{(0)}_{x}$ propagate along the same direction. Thus the distinguishable PPF from the BPF would be only $N^{(1)}_{x\,\mathrm{II}}$, but not $N^{(1)}_{x\,\mathrm{I}}$. Utilizing similar means it can be shown that in the 1st, 2nd, 3rd and 4th octants, the distinguishable PPF from the BPF will be one kind of the PPFs, namely, $N^{(1)}_{x\,\mathrm{I}}$ or $N^{(1)}_{x\,\mathrm{II}}$. Consequently, role of the fractal membranes looks like a "one-way valve" with strong focusing function to the photon flux in the GHz band. This property will be very useful to distinction and displaying the PPFs generated by the stochastic HFRGW background.

Of course, if considering other possible noise sources and diffraction effects, the values listed in Table 1 will be further reduced; thus, an obvious gap still exists between the theoretical schemes and reality.

6 Thermal noise and EM noise

At the moment there are no operating prototypes of the EM detecting system, although relevant researches and construction of the EM detecting system are already in progress; it is difficult to give a complete description for the noise issues. However, since our purpose is the display and detection of the PPF of about $\nu = 5\,\mathrm{GHz}$ in the terminal microwave receiver, our attention will be focused onto two key aspects.

(1) What are strength and physical behavior of the PPF (signal) and the BPF (background) reaching the microwave receiver?
(2) How could one distinguish the PPF and other photons caused by noise, such as thermal noise, background noise and external EM noise?

Here we shall give a very brief and rough review.

Except for the background photon noise issue just mentioned, there are the thermal noise sources and possible external EM noise sources. Because the frequency of the PPF (signal) is roughly 5 GHz, if the system is cooled down to $k_{\mathrm{B}}T < \hbar\omega_e$ (k_{B} is Boltzmann's constant, $\omega_e = 2\pi\nu_e$, $\nu_e = 5\,\mathrm{GHz}$), i.e., $T < \hbar\omega_e/k_{\mathrm{B}} \sim 0.24\,\mathrm{K}$, then the frequency ν_m of the thermal photons will be less than the ν_e of the PPF. If the apparatus is kept to a lower temperature, e.g., $T < 0.024\,\mathrm{K}$ or 24 mK (this is well within the current technology), then we have $\nu_m \approx 10^{-2}\nu_e$. Thus the difference in the frequency band for two such kinds of photons would be very great, i.e., the signal photon flux and the thermal photons can easily be distinguished. In other words, practically speaking there are no thermal photons at 5 GHz, and in this way the thermal noise can be suppressed as long as the EM detector can select the correct frequency. Note that the low temperature is very convenient for the operation of the superconductors and the strong static magnetic field.

For the possible external EM noise sources, using Faraday cage or shielding covers made from such fractal membranes [57–59] or from a tight mosaic of superconductor chips on the inside surface of the detector's cryogenic containment vessel would be very effective. Moreover, a good "microwave darkroom" can provide an effective shielding environment, and in this case possible dielectric dissipation (using a vacuum operation) can be effectively suppressed. In this case one would obtain a suitable environment for a measurable signal-to-noise ratio.

Also, the superposition of the relic GW stochastic components will cause a fluctuation of the PPFs, even if such "monochromatic components" all satisfy the frequency resonant condition ($\omega_e = \omega_g$). However, (59), (61), (64), (67) and (68) show that the metric perturbation only influences the strength fluctuation of the PPFs and does not influence the "direction resonance". That is, it does not influence the selection capability of the EM system to the propagating directions of the relic GWs, and it does not influence average effect over time of the PPFs.

In addition, the values of the PPFs discussed in the present paper depend on the strength of the HFRGWs in the GHz band expected by the QIM and other relevant string cosmology scenarios (see, e.g., [1–7]). Because such models and scenarios are somewhat controversial, we cannot know in advance how accurate these models and scenarios might be. If the strength of the real HFRGWs in the GHz band are much less than the magnitude expected by such models and scenarios, even if the required conditions can be satisfied, one might still not be able to detect and measure such HFRGWs; then the HFRGW models will be corrected. Thus, this scheme might provide an indirect way to test such models and scenarios; that is, as suggested by Brustein et al. [64], a null experiment would be valuable. In any event, the HFGW generator and detector experiment described in [9, 10], which operate at about the same frequencies as the HFRGWs, will prove the concept of the present detector independently from cosmological experiments.

Moreover, there are some issues and problems that need further investigation. For example, how to generate a typical and high-quality GB, how to suppress distortion of the spot radius of the GB and align it, what is concrete correction to the PPF caused the higher-order modes of the GB, how to further estimate and analysis the relevant noise sources, what are concrete influence and correction of the fractal membranes (or plates) to the GB itself, how to estimate and effectively suppress diffraction effect by new materials (e.g. the fractal membranes), how to ensure

a good vacuum to avoid the scattering of photons and dielectric dissipation caused by the dust and other particles, etc. All these issues and problems need careful theoretical and experimental study. A more detailed investigation concerning such issues will be the object of further research and will be studied elsewhere.

7 Concluding remarks

1. Although the usual analytic expressions of the relic GWs are often complicated, the high-frequency asymptotic behavior of them in the microwave band can be expressed as simpler forms, and they can be described as a superposition of all quasi-monochromatic components. The energy density of the HFRGWs is positive definite, and their momentum densities have reasonable physical behavior, the EM resonant response of the HFRGWs in the laboratory frame of reference can be treated as resonance interaction of the quasi-monochromatic HFGWs with the EM fields.
2. Under synchro-resonance conditions, coherent modulation of the HFRGW to the preexisting transverse BPFs would produce the transverse PPFs, the PPFs propagating along two orthogonal directions of the double transverse polarized electric modes of the GB are generated by the pure $\otimes$ polarization and the pure $\oplus$ polarization states of the HFGW, respectively. The former has a maximum at the longitudinal symmetrical surface of the GB, where the transverse BPF vanishes, but the latter and the BPF have the same distribution. Thus, the former may provide an observable effect, while the latter will be swamped by the BPF.
3. The PPF reflected or transmitted by the fractal membranes exhibits a very small decay compared with the much stronger BPF. In our case this is the PPF produced by the pure $\otimes$ polarization state of the HFGW. Another interesting area would be the region in which the PPF and the BPF might reach a comparable order of magnitude.
4. Although an obvious gap still exists between the theoretical estimation and reality, there are is potential space to advance and there are new ways [65–68] to further improve the sensitivity and the detecting ability of the EM system. These new ways and technology will include generation of super-strong static magnetic fields (e.g., use of crystal channel effect), ultra-high sensitivity microwave single photon detectors such as a circuit with quantum electrodynamics device (CQED) photon detectors, a Rydberg atom cavity detector, a SQUID array mux, Josephon junction arrays, etc., and possible optimized combinations of them. They possibly lead to further narrowing of such a gap and provide new promises.

Acknowledgements. This work is supported by the National Basic Research Program of China under Grant No. 2003 CB 716300, the National Natural Science Foundation of China under Grant No. 10575140, the Foundation of China Academy of Engineering Physics under Grant Nos. 2008 T 0401, 2008 T 0402, the Nature Science Foundation of Chongqing under Grant No. 8562, GRAVWAVE® LLC, Transportation Sciences Corporation and Seculine Consulting of the USA.

References

1. M. Giovannini, Phys. Rev. D **60**, 123 511 (1999)
2. M. Giovannini, Class. Quantum Grav. **16**, 2905 (1999)
3. A. Riazuelo, J.P. Uzan, Phys. Rev. D **62**, 083 506 (2000)
4. J.E. Lidsey et al., Phys. Rep. **337**, 343 (2000)
5. E.J. Copeland et al., gr-qc/9803070
6. M. Gasperini, G. Veneziano, Phys. Rep. **373**, 1 (2003)
7. G. Veneziano, Sci. Am. **290**, 30 (2004)
8. G.S.B. Kogan, V.R. Rudenko, Class. Quantum Grav. **21**, 3347 (2004)
9. R.M.L. Baker Jr., F.Y. Li, AIP Conf. Proc. **813**, 1249 (2006)
10. R.M.L. Baker Jr., C.R. Woods, F.Y. Li, AIP Conf. Proc. **813**, 1280 (2006)
11. P. Chen, Mod. Phys. Lett. A **6**, 1069 (1991)
12. N.A. Hamed, S. Dimopoulos, G. Dvali, Sci. Am. **238**, 62 (2000)
13. M.E. Gertsenshtein, Sov. Phys. JETP **14**, 84 (1962)
14. W.K. De Logi, A.R. Mickelson, Phys. Rev. D **16**, 2915 (1977)
15. V.B. Braginsky, M.B. Mensky, JETP Lett. **13**, 417 (1971)
16. L.P. Grishchuk, M.V. Sazhin, Sov. Phys. JETP **41**, 787 (1975)
17. L.P. Grishchuk, M.V. Sazhin, Sov. Phys. JETP **53**, 1128 (1983)
18. L.P. Grishchuk, Paper-HFGW-119, In: High-Frequency Gravitational Wave Conference, ed. by P. Murad, R.M.L. Baker Jr. (MITRE Corporation, Mclean, VA, USA, 2003)
19. U.H. Gerlach, Phys. Rev. D **46**, 1239 (1992)
20. M.V. Mitskienich, A.I. Nesterov, Gen. Relat. Grav. **27**, 361 (1995)
21. F.Y. Li, M.X. Tang, D.P. Shi, Phys. Rev. D **67**, 104 008 (2003)
22. F.Y. Li, M.X. Tang, D.P. Shi, Paper HFGW-03-108, In: High-Frequency Gravitational Wave Conference, ed. by P. Murad, R.M.L. Baker Jr. (MITRE Corporation, Mclean, VA, USA, 2003)
23. F.Y. Li, M.X. Tang, J. Luo, Phys. Rev. D **62**, 044 018 (2000)
24. M.X. Tang, F.Y. Li, Class. Quantum Grav. **17**, 2447 (2000)
25. F.Y. Li, M.X. Tang, Int. J. Mod. Phys. D **11**, 1049 (2002)
26. F.Y. Li, R.M.L. Baker Jr., Int. J. Mod. Phys. B **21**, 3274 (2007)
27. F.Y. Li, Y. Chen, P. Wang, Chin. Phys. Lett. **24**, 3328 (2007)
28. D. Boccaletti et al., Nuovo Cim. B **70**, 129 (1970)
29. T. Tokuoka, Prog. Theor. Phys. **54**, 1309 (1975)
30. J.B. Griffiths, J. Phys. A **16**, 1175 (1983)
31. D. Papadopoulos et al., Astron. Astrophys. **377**, 701 (2001)
32. M. Servin, G. Brodin, gr-qc/0302039
33. A.M. Cruise, Class. Quantum Grav. **17**, 2525 (2000)
34. M. Cruise, R.M.J. Ingley, Class. Quantum Grav. **22**, S479 (2005)

35. P. Bernard et al., Rev. Sci. Instrum. **72**, 2428 (2001)
36. P. Bernard et al., gr-qc/0203024
37. A. Chincarini et al., Paper HFGW-03-103, In: High-Frequency Gravitational Wave Conference, ed. by P. Murad, R.M.L. Baker Jr. (MITRE Corporation, Mclean, VA, USA, 2003)
38. R. Ballantini et al., Class. Quantum Grav. **20**, 3505 (2003)
39. L.P. Grishchuk, gr-gc/0002035
40. L.P. Grishchuk, gr-gc/0305051
41. L.P. Grishchuk, gr-gc/0504018
42. N.N. Gorkavyi, Paper HFGW-03-115, In: High-Frequency Gravitational Waves Conference, ed. by P. Murad, R.M.L. Baker Jr. (MITRE Corporation, Mclean, VA, USA, 2003)
43. Y. Zhang, Y. Yuan, W. Zhao, Y.T. Chen, Class. Quantum Grav. **22**, 1383 (2005)
44. L. Randall, R. Sundrum, Phys. Rev. Lett. **83**, 3370 (1999)
45. L. Randall, R. Sundrum, Phys. Rev. Lett. **83**, 4690 (1999)
46. R.M.L. Baker Jr., P.A. Murad, Paper AIAA 2003-4882, In: AIAA/ASME/ASEE, Joint Propulsion Conference and Exhibit, Huntsville, Alabama, American Institute of Aeronautics and Astronautics, 2003
47. I. Osborne et al., Science **296**, 1417 (2002)
48. C. Serife, Science **305**, 464 (2004)
49. M. Livio, M.J. Rees, Science **309**, 1022 (2005)
50. C.J. Hogan, Am. Sci. **90**, 420 (2002)
51. L.P. Grishchuk, M. Soloklin, Phys. Rev. D **43**, 2566 (1991)
52. Y. Zhang, X.Z. Er, T.Y. Xia, W. Zhaoand, H.X. Miao, Class. Quantum Grav. **23**, 3783 (2006)
53. Y. Zhang, H.X. Maio, Phys. Rev. D **75**, 104 009 (2007)
54. M. Giovannini, Phys. Rev. D **73**, 083 305 (2006)
55. N. Rosen, K.S. Virbhadra, Gen. Relat. Grav. **25**, 429 (1993)
56. A. Yariv, Quantum Electronics 2nd ed. (Wiley, New York, 1975)
57. W.J. Wen et al., Phys. Rev. Lett. **89**, 223 901 (2002)
58. L. Zhou et al., Appl. Phys. Lett. **82**, 1012 (2003)
59. B. Hou et al., Opt. Express **13**, 9149 (2005)
60. S.R. Sechadri, J. Opt. Am. A **18**, 1748 (2001)
61. S.R. Sechadri, J. Opt. Am. A **16**, 1373 (1999)
62. E.G. Bessonov, physics/9802037
63. V. Sabbata, D. De Boualetti, C. Gauldi, Sov. J. Nucl. Phys. **8**, 537 (1969)
64. R. Brustein et al., Phys. Lett. B **361**, 45 (1995)
65. D.I. Schuster et al., cond-mat/0608693
66. K. Yamarnoto et al., hep-ph/0101200
67. W.J. Kim, J.H. Brownell, R. Onofrio, Phys. Rev. Lett. **96**, 200 402 (2006)
68. P. Chen, Resonant Photon–Graviton Conversion in EM Fields: From Earth to Heaven, Stanford Linear Accelerator Center-PUB-6666, September, 1994
69. W.J. Wen, private communication (2007)